Open access • Journal Article • DOI:10.1039/C3EE43525C

Energy storage applications of activated carbons: supercapacitors and hydrogen storage — Source link

Marta Sevilla, Robert Mokaya

Institutions: Spanish National Research Council, University of Nottingham

Published on: 21 Mar 2014 - Energy and Environmental Science (The Royal Society of Chemistry)

Topics: Hydrogen storage and Hydrogen economy

Energy storage applications of activated carbons: supercapacitors and hydrogen storage

Marta Sevilla[a*], Robert Mokaya[b*]

[a] Instituto Nacional del Carbón (CSIC), P.O. Box 73, 33080 Oviedo, Spain

[b] School of Chemistry, University of Nottingham, University Park, Nottingham NG7 2RD, U. K.

[*] Corresponding author. Fax: +44 115 9513562. E-mail address: r.mokaya@nottingham.ac.uk (R. Mokaya); Fax: +34 985 29 76 62; E-mail address: martasev@incar.csic.es (M. Sevilla)

Abstract

Porous carbons have several advantageous properties with respect to their use in energy applications that require constrained space such as in electrode materials for supercapacitors and as solid state hydrogen stores. The attractive properties of porous carbons include, ready abundance, chemical and thermal stability, ease of processability and low framework density. Activated carbons, which are perhaps the most explored class of porous carbons, have been traditionally employed as catalyst supports or adsorbents, but lately they are increasingly being used or find potential applications in the fabrication of supercapacitors and as hydrogen storage materials. This manuscript presents the state-of-the-art with respect to the preparation of activated carbons, with emphasis on the more interesting recent developments that allow better control or maximization of porosity, the use of cheap and readily available precursors and tailoring of morphology. This review will show that the renewed interest in the synthesis of activated carbons is matched by intensive investigations into their use in supercapacitors, where they remain the electrode materials of choice. We will also show that activated carbons have been extensively studied as hydrogen storage materials and remain a strong candidate in the search for porous materials that may enable the so-called Hydrogen Economy, wherein hydrogen is used as an energy carrier. The use of activated carbons as energy materials has in the recent past and is currently experiencing rapid growth, and this review aims to present the more significant advances.

Broader Context

In order to meet the growing energy demands required to sustain current living standards whilst at the same time avoiding resource depletion and environmental pollution, there is a need for the development of high-performance, low cost and environmentally-friendly energy storage and production systems. Suitable materials are key ingredients enabling the search for new energy systems. Much current research effort is focused on improving the performance of energy storage devices such as supercapacitors and batteries (e.g., Li-ion batteries), and hydrogen storage systems that may enable the use of hydrogen as an energy carrier in fuel cells for the proposed Hydrogen Economy. Activated carbons are one of the most studied classes of materials for applications in these two important research areas, as electrode materials in supercapacitors and solid state hydrogen stores. In this review we present the state-of-the-art with respect to the preparation of activated carbons and consider recent developments in their use in supercapacitors, where they remain the electrode materials of choice. We also review the burgeoning research area of activated carbons as hydrogen storage materials and suggest that they remain strong candidates in the search for porous materials that may enable the anticipated Hydrogen Economy.

1. Introduction

Meeting the growing energy demand of the current society, while avoiding resource depletion and environmental pollution, requires the development of high-performance, low cost and environmentally-friendly energy storage and production systems. Currently much research effort is focused on the improvement of the performance of energy storage devices, such as supercapacitors and batteries (especially Li-ion batteries), and energy production systems such as fuel cells. In order to accomplish such target, a key aspect is the design of novel materials and development of synthesis processes that allow a precise control over the structural and chemical characteristics of the material, as well as seeking greener and cost effective material synthesis processes for the widespread utilization of such devices.

Carbon-based materials have attracted considerable interest in many energy-related applications due to their abundance, chemical and thermal stability, processability and the possibility of tuning their textural and structural characteristics to fulfill the requirements of specific applications. In particular, activated carbons stand out for their large surface area (> 1000 m^2/g) and pore volume (> 0.5 cm^3/g), and relatively low cost. Thus, they have a long history as adsorbents for the removal of impurities from gases and liquids.[1] The first industrial production processes of activated carbons with defined properties were developed at the beginning of the 20^{th} century, with powder forms. Later on, the need to develop protective gas masks during World War I, promoted the development of granular activated carbon. Currently, activated carbons are available in other physical forms such as fibers, pellets, cloths or felts in order to satisfy advancing industrial technological needs. As well as the various physical forms, there have been many advances in the control of the textural characteristics of activated carbons. Thus, whereas traditional activated carbons are

characterized by a broad pore size distribution (PSD) covering the micropore to the macropore region, recent developments in activation procedures and/or precursors allow a better control over the pore size distribution, as will be described in detail in this review. These characteristics have widened the usefulness of activated carbons to more demanding applications, such as catalysis/electrocatalysis, energy storage in supercapacitors and Li-ion batteries, CO_2 capture or H_2 storage. This review will cover the energy-related applications of activated carbons, with a summary of recent research progress on the development of activated carbons with more controlled structural and chemical characteristics. It should be pointed out that, although other porous materials exhibit a more controlled porosity, such as templated carbons, carbide-derived carbons (CDCs) or metal organic frameworks (MOFs), the simplicity and well-established production methods of activated carbons means that they continue to be the main candidates for many energy applications.

2. Preparation of Activated Carbons (ACs)

2.1. Activation methods

The activation of carbon materials can be performed in two ways: i) physical activation with different oxidizing gases, such as air, O_2, CO_2, steam or their mixtures, and ii) chemical activation with KOH, NaOH, H_3PO_4 or $ZnCl_2$, among other chemical compounds. The physical activation process is a two-step process, where pyrolysis in an inert atmosphere (usually nitrogen) of the precursor normally at 400-900ºC is performed before the partial gasification using an oxidizing gas at 350-1000°C to develop the porosity and surface area. On the contrary, the chemical activation process is a one-step process, where the activating agent (typically an acid, strong base or a salt) is incorporated into the carbon precursor prior to pyrolysis at a temperature of 450-900ºC. The combination of both physical and chemical processes is also possible.

A wide range of organic products is suitable as feedstock for the manufacture of activated carbon. Agricultural and forest biomass such as wood, sawdust, peat, coconut shells, fruit bones or rice husk are the preferred uncarbonized feedstocks.[2,3,4,5,6] The use of such materials is really attractive as they are abundant and low-cost wastes which can be converted in high value-added products. With regards to carbonized feedstocks coal, low temperature lignite coke, charcoal or biochar are utilized.[7,8] The properties of the activated carbons depend much on the type of feedstock utilized. With the development of new forms of carbon, such as nanotubes, nanofibers, templated carbons or carbide-derived carbons (CDCs), their post-synthesis activation has also been explored as a way of enhancing their porous characteristics.[9,10,11,12,13]

2.1.1. Physical activation

As previously mentioned, in the physical activation process, a carbon precursor is first exposed to pyrolysis in an inert atmosphere at 400-900ºC to eliminate the bulk of volatile matter, followed by partial gasification using an oxidizing gas at 350-1000°C. Initially, the active oxygen in the activating agent burns away the tarry pyrolysis off-products trapped within the pores, leading to the opening of some closed pores. Then the microporous structure is developed as the oxidizing agent burns away the more reactive areas of the carbon skeleton resulting in CO and CO_2, with the extent of burn-off depending upon the nature of the gas employed and the temperature of activation. CO_2, air and steam are used as activating agents. The chemical and physical nature of physically activated carbons is very dependent on the precursor, the oxidizing agent employed, the temperature of activation and the degree of activation. Depending on these factors, activated carbons with moderate to high porosity can be achieved, as well as with varying surface chemistry (i.e. amount and type of oxygen groups). As a general trend, the higher the activation temperature/activation time, the larger the porosity

development. However, higher porosity developments are usually accompanied by a broadening of the pore size distribution (PSD).

When air (or oxygen) is used as the activating agent, problems are encountered due to the exothermic nature of the reaction of carbon with air (oxygen). The speed of this reaction makes it difficult to control the process, resulting in excessive burn-off and reducing the activated carbon yield. However, the high reactivity of oxygen makes the process low energy/cost, as it requires lower activation energy compared to the use of steam or CO_2,[14,15] and therefore, it has been used by different groups. Thus, Feng and Bathia studied the variation of pore structure of several coal chars during gasification in air and carbon dioxide.[16] Gasification in air of the chars (coals pyrolyzed at 900-1150ºC) was performed at 380ºC, whereas CO_2 gasification was done at 800ºC. They observed that in air gasification, the surface area and pore volume initially increase rapidly and then slowly with carbon conversion. The surface area and volume of the small micropores (< 1 nm) does not change significantly with carbon conversion after a certain level of conversion, whereas those in the 1-2 nm and 2-5 nm range increase with conversion (see Figure 1a). On the other hand, for CO_2 gasification, the surface area and volume of small micropores increase dramatically with the progress of gasification, and for the other pore size ranges also an increase is observed with conversion. Materials with surface area up to ~ 700 m^2/g and pore volume up to ~ 0.55 cm^3/g were obtained for air gasification, whereas for CO_2 values up to 500 m^2/g and ~ 0.22 cm^3/g were measured. Gañán et al. prepared activated carbons, from almond tree pruning, with surface area up to 560 m^2/g and pore volume below 0.31 cm^3/g by air gasification at 190-260ºC, both parameters increasing with increase of gasification temperature and time.[17] More recently, Osswald et al. performed the activation of advanced materials, such as TiC-derived carbide-derived carbons (TiC-CDCs), with air and CO_2.[18] They

observed a rise in surface area and pore volume with increase of activation time and temperature in the air gasification process. However, the increase was moderate (~ 10%) and accompanied by a large weight loss. Additionally, the high reactivity of O_2 led to a rapid enlargement of micropores into mesopores. With regards to CO_2, the surface area and pore volume followed the same trend as for air, though the increase was in this case remarkable, up to 77% for the surface area, whereas the pore volume was almost doubled. Thus, a surface area of ~ 3100 m^2/g and pore volume of 1.3 - 1.4 cm^3/g was achieved by activation at 950ºC for 2h. The average pore size shifted towards higher values with increasing activation time and temperature. Furthermore, they successfully applied the same procedure to other CDCs, such as SiC-CDC.

Steam and CO_2 are preferred to air as activating agents due to the reasons discussed above. There is general agreement that steam is a more reactive agent than CO_2 and therefore requires the application of lower temperatures.[11,19,20] The surface area, pore volume and average pore diameter of the resulting activated carbon generally increases with the extent of burn-off in both gasifying agents.[16,17,18,20,21,22,23,24,25,26,27,28] However, contradictory information has been published regarding the type of porosity generated by each activating agent. Some authors have reported that steam activation produces carbons with a narrower and more extensive micropore structure than CO_2,[20,22,23,24,29] whereas others observed that comparatively lower micropore volumes but larger external surface areas were produced in steam-activated carbons.[21,25,26,27,28] Nevertheless, materials with surface area lower than 1800 m^2/g and pore volumes up to ~ 0.9 cm^3/g are normally obtained.[11-29]

2.1.2. Chemical activation

The chemical activation process consists of the heat-treatment of a mixture of the carbon precursor and the activating agent at a temperature normally in the 450-900ºC

range. It has the following advantages over physical activation: i) usually involves only one step, ii) lower pyrolysis temperatures are used, iii) much higher carbon yield is obtained, iv) materials with very high surface area (~ 3600 m^2/g) can be produced and v) the microporosity can be well developed, controlled and tailored to be narrowly distributed. These last two strengths of the chemical activation process are very important for applications such as energy storage in supercapacitors or gas (H_2, CH_4 or CO_2) storage, which demand materials with large surface areas and a microporosity adjusted to the size of the electrolyte ions for supercapacitors or ~ 0.7 – 1 nm for gas storage.[30,31,32,33,34,35,36,37,38,39,40]

Of the many reagents proposed for chemical activation ($ZnCl_2$, H_3PO_4, $AlCl_3$, $MgCl_2$, KOH, NaOH, etc.), $ZnCl_2$, H_3PO_4 and KOH are the most commonly used. $ZnCl_2$ and H_3PO_4 act as dehydrating agents, whereas KOH acts as oxidant. As observed by Jagtoyen and Derbyshire,[41] H_3PO_4 promotes dehydration at a lower temperature than does thermal treatment alone, and the evolution of CO and CO_2 commence at a lower temperature. During the heat treatment, the activating agent present in the interior of the particles produces a dehydrating effect on the carbon precursor. It is presumed that, during this dehydrating step, cross-linking reactions (cyclization and condensation processes) are predominant. The dehydration of the carbon precursor causes a reduction in the dimensions of the particle, although such reduction is partially inhibited because the activating agent remains within the particle during the thermal treatment, thus acting as template for the creation of microporosity. In addition, H_3PO_4 combines with organic species forming phosphate and polyphosphate bridges that connect biopolymer fragments, thereby partially hindering the contraction in the material as the temperature increases. Heterogeneity in the microporosity is observed, which is mostly independent of the amount of H_3PO_4 used, and it is due to the fact that during activation there are no

phosphoric acid molecules, but a mixture of molecules (i.e., H_3PO_4, $H_4P_2O_5$, $H_{13}P_{11}O_{34}$).[42] On the other hand, in the case of $ZnCl_2$, the small size of the $ZnCl_2$ or its hydrates leads to small and uniform size micropores.[42] On the contrary, as shown by Linares-Solano and co-workers,[43,44,45] KOH and NaOH do not act as dehydrating agent, but as oxidant. In this case, a redox reaction takes places as follows: $6KOH + 2C \leftrightarrow 2K + 3H_2 + 2K_2CO_3$. The carbon framework is etched to generate pores due to the oxidation of the carbon into carbonate ions and intercalation of the resulting potassium compounds, which are removed during subsequent washing steps. On the other hand, the production of CO_2 from the decomposition of K_2CO_3 at temperatures above 700°C can contribute to further porosity development through carbon gasification.[46] Several studies have shown that the higher the reactivity of the precursor, the lower the temperature required to trigger gassification,[47,48] the higher the degree of gasification caused by the CO_2 evolved from K_2CO_3 and the larger the resultant porosity development.[44]

In general, as the amount of activating agent increases, the porosity development (surface area and pore volume) is greater, but this is accompanied by a widening of the PSD (see Figures 1b – 1c).[40, 49, 50] Initially, the development of porosity is centered in the microporosity. With increase in the amount of activating agent, the PSD becomes more heterogeneous, with observable differences dependent on the nature of activating agent. Thus, Molina-Sabio and Rodríguez-Reinoso observed that activation of peach stones with KOH only produces widening of the microporosity to more heterogeneous micropores, whereas $ZnCl_2$ develops both wide micropores and low mesopores, and H_3PO_4 develops large mesopores and even macropores.[51] With regards to the influence of the activation temperature, many authors have found that there is an optimum temperature for porosity development, which depends on the activating agent and the

carbon precursor. Thus, the porosity increases with the temperature to a maximum and then begins to decrease with further increase of the temperature due to shrinkage or collapse of the structure.[41, 46, 52,53,54,55] In this sense, several studies show that increase in temperature above 500ºC for chemical activation with $ZnCl_2$ or H_3PO_4 may induce not only a weight loss but also shrinkage in carbon structure, leading to a reduction, as well as narrowing, in porosity. The structural contraction above 500ºC suggests that cross-links formed at low temperatures by treatment with $ZnCl_2$ or H_3PO_4 do not have a high thermal stability with the consequent breakdown and rearrangement of carbonaceous aggregates and the collapse or shrinkage of pores.[41, 52, 54, 55] For KOH, the maximum porosity development is achieved at higher temperatures (700 - 900ºC), which suggests that cross-links induced by KOH activation are more thermally stable than those derived from $ZnCl_2$ or H_3PO_4 treatment.[46,55] As mentioned above, the larger porosity development with the increase of the activation temperature is normally accompanied by a widening of the PSD. Hsu and Teng observed that, for activation with $ZnCl_2$ and H_3PO_4, the carbonization temperature does not have a significant influence on the PSD, the proportion of micropore volume varying within 80-90%.[55] Tsai et al. have found similar results for activation with $ZnCl_2$ [53] and Teng et al. and Puziy et al. for activation with H_3PO_4.[52, 56] However, for KOH, Hsu and Teng found a pronounced effect of the temperature on the PSD.[55] This has been corroborated by the results of many authors, which show that the activation temperature is a key factor in controlling the PSD.[40,46,57,58, 59,60,61,62] This is due to the fact that from 500 to 700ºC, the formation of micropores takes place due to the release of volatiles. However, above 700ºC, the release of CO_2 from K_2CO_3 formed during carbonization becomes significant and carbon gasification takes places, opening up closed pores and enlarging existing micropores, which results in a broadening of the PSD (see Figure 1d). Additionally,

metallic potassium is formed, which then intercalates within the graphite-like laminar structure, widening the spaces between carbon atomic layers and increasing the pore volume.[46,63] Other parameters that affect the porosity development are (i) the mixing procedure (solution or mechanical mixing), (ii) activation time, (iii) gas flow rate, (iv) type of gas used during the heat-treatment and (v) heating rate.[46,57,58,64,65,66]

Among the various activating agents, KOH generates activated carbons with extremely large surface area up to ~4000 m^2/g), high pore volume up to 2.7 cm^3/g, [40,46,55,57,59,64,67,68,69,70,71,72,73,74,75] and tunable and narrow PSD through the control of the activating conditions (i.e., temperature and amount of KOH),[40,61,64,71,74,75, 76] as is described below. For other activating agents, the surface areas are normally between 1500 and 2000 m^2/g with pore volume < 1.5 cm^3/g and broad PSD. [52,53,55,56,77,78]

2.1.3. Combination of physical and chemical activation processes

Two stage activation processes consisting of a chemical activation step (normally with H_3PO_4 or $ZnCl_2$) followed by physical activation (usually with CO_2) have also been used to further enhance the porosity development and tune the PSD of activated carbons. Thus, Hu et al. applied CO_2 activation at 800ºC to $ZnCl_2$ or KOH activated carbons prepared from coconut shells and palm stones with the aim of increasing the mesoporosity.[79] In such a way, materials with surface areas up to ~ 2400 m^2/g and 14-94% of mesoporosity were obtained. Later on, Prauchner and Rodríguez-Reinoso employed a combination of chemical activation with H_3PO_4 or $ZnCl_2$ with CO_2 activation at 750ºC over coconut shell to synthesize activated carbons with textural characteristics applicable to natural gas storage.[80] The use of small amounts of chemical reagent allowed the generation of narrow microporosity without inducing significant reduction of bulk density, whereas the subsequent step of physical activation permitted the appropriate development of the primary pore structure generated in the chemical

activation step. Very recently, Arami-Niya et al. followed the same procedure as Prauchner and Rodríguez-Reinoso over oil palm shell, and targeted activated carbons with textural characteristics suitable for methane storage.[81] Other examples where a combination of chemical and physical activation has been used are available.[82,83,84] It is worth mentioning the example of Hu and Srinivasan, where physical activation with CO_2 was used simultaneously with chemical activation with $ZnCl_2$.[85] Thus, coconut shell or palm seed were impregnated with $ZnCl_2$, dehydrated overnight at 110ºC and heat-treated under N_2 up to 800ºC; once the temperature was reached, N_2 was replaced by CO_2 and maintained for 2-3 h. Additionally, the authors compared the textural characteristics of such materials to those obtained by sequential chemical-physical activation using the same experimental conditions. They observed that simultaneous activation yielded activated carbons with both high surface area and high mesopore content, whereas sequential activation generated less mesoporosity, which suggests that evaporation of $ZnCl_2$ (boiling point = 732ºC) is more effective in removing $ZnCl_2$ than via a washing step.

2.2. Activated carbons with ultra-high surface areas

Among the various activating agents, KOH allows the synthesis of activated carbons with the highest surface areas (up to ~4000 m^2/g) whilst still maintaining narrow PSD. Furthermore, the PSD of KOH activated carbons can be tuned through the control of the activating conditions. Thus, Lozano-Castelló et al. showed the possibility of generating highly porous materials (surface area > 2000 m^2/g) with homogeneous micropore size distribution from coal precursors (anthracite and bituminous coal) by the careful selection of the activation conditions (KOH/precursor ratio, gas flow and impregnation method).[64] It should be emphasized that this type of microporosity cannot be obtained by other activation methods where the increase in surface area is accompanied by pore

widening.

The most widely known high surface area KOH-activated carbon is MAXSORB, produced from a petroleum coke. It was developed in the 1970s by the AMOCO Corporation (termed PX-21)[86,87] and commercialized by the Anderson Development Company in the mid-80s in the USA (as AX-21). Further development of this material was carried out by The Kansai Coke and Chemical Company Ltd, who commercialise it as MAXSORB.[88] This activated carbon is characterized by a BET surface area of ~ 3100 m^2/g and a pore volume of 1.7 cm^3/g, which is made up of micropores-supermicropores (mean pore diameter = 2.12 nm[89]), as shown in Figure 2a. Figure 2b further evidences that it is a relatively homogeneous carbon, where the walls of the pores are formed by only one or two layers of carbon atoms. Owing to these characteristics, the behavior of such carbon material has been analyzed in a variety of applications, such as the recovery of chlorinated hydrocarbon solvent vapor,[89] hydrogen storage,[90] methane storage,[91,92] CO_2 adsorption,[93] catalyst or catalyst support[94,95] and supercapacitors.[96,97]

Recently, KOH activation has gained increasing attention as it has proved to be a powerful technique for the generation of carbon materials with ultrahigh surface areas (> 2500-3000 m^2/g) from a variety of carbon materials, including non-porous substances, such as hydrothermally carbonized carbons[61,62,98] or polymers,[40,99,100] to advanced porous materials such as CDCs,[33,76,101,102] zeolite-templated carbons (ZTCs),[13] silica-templated carbons[103,104] or graphene.[105] The extremely high porosity development translates to an enhancement in hydrogen or methane storage, CO_2 capture or energy stored when used as electrodes in supercapacitors. Although most high surface area activated carbons are generated by KOH activation, CO_2 physical activation or H_3PO_4 chemical activation of suitable carbon precursors can lead to materials with large

surface areas. Thus, Gogotsi et al. have synthesized activated carbons with surface area up to ~3400 m^2/g via CO_2-activation of carbide-derived carbons.[18,33,101] On the other hand, Wang et al. achieved surface area of 2700 m^2/g by H_3PO_4 chemical activation of hydrothermally carbonized rice husk.[106]

A comparison of the highest surface area reported up to date for different porous materials is shown in Figure 3. It can be seen that only some metal-organic frameworks (MOFs),[107,108] covalent organic frameworks (COFs)[109,108] and porous polymers[110,108] exhibit higher surface area than KOH-activated carbons. However, it should be noted that, although there is one porous polymer with surface area of 5640 m^2/g (PAF-1),[110] normally they exhibit BET surface areas lower than 2000 m^2/g.[108] On the other hand, some of the most porous examples of MOFs and COFs possess limited physicochemical stability, whereas activated carbons are highly stable.

2.3. Activated carbons monoliths

For the practical application of activated carbons as sorbents or storing media, not only the mass adsorption/storage capacity is important, but also the volumetric capacity may be a key parameter, especially when space constrictions are a bottle neck, as in mobile applications. In such cases, conforming of the activated carbons in pellets or monoliths to increase the packing density is essential, especially for highly activated carbons, whose density can be extremely low. Pellets and monoliths can additionally be easier to handle compared to powders and their use is essential for preparing supercapacitors or batteries electrodes. Activated carbons have the advantage that can be compacted into monoliths or pellets without the use of a binder by the appropriate selection of the carbon precursor and preparation method with the advantage that: i) the synthesis process involves less steps, ii) no loss of porosity due to the presence of binder,[111] and iii) no increase in electrical resistivity due to the presence of a binder, which is an

important consideration for electrochemical applications.[112] Several examples of the formation of monoliths of activated carbons using a polymer or pitch binder are available.[113,114,115,116,117,118] A strategy followed by some authors to unblock part of the porosity occluded by the binder is via an additional activation step performed on the monolith.[118] The synthesis procedures used by different authors to prepare activated carbon monoliths with and without the aid of a binder are depicted in Figure 4.

Inomata et al. demonstrated the synthesis of binderless monoliths of activated carbon from compacted cellulose.[119] In a first step, cellulose microcrystal powder was pressed into monoliths (Figure 5a) and afterwards carbonized at 800ºC. Finally, the monoliths were subjected to a physical activation process with CO_2 at 800-900ºC (Figure 5b). As a result, carbon monoliths with bulk densities in the 0.56–0.99 g/cm^3 range were obtained, values which are ~2–4 times higher than that of activated carbon powder. The bulk density increased with compaction pressure, whereas the true density (1.9 g/cm^3) was independent of the compaction pressure. However, the increase of the compaction pressure was detrimental to porosity development; the pore volume and surface area decreased at higher compaction pressure from 1790 m^2/g and 0.74 cm^3/g to 1100 m^2/g and 0.46 cm^3/g, respectively. The compacted carbons exhibited a methane storage capacity of up to 164 v/v at 35 bar vs. ~ 75 v/v for activated carbon powder. A similar procedure was successfully applied to activated carbon monoliths derived from coconut shell, peach stones and coffee beans, which achieved bulk density in the range 0.60-0.88 g/cm^3.

Molina-Sabio et al. prepared binderless activated carbon discs from olive stones by chemical activation with H_3PO_4[120] or $ZnCl_2$.[121] In this case, the compaction step consisted of hot compression (up to 300ºC) and was performed between impregnation with the chemical agent and heat-treatment. The bulk density of the prepared disc was

higher than for granular carbons due to a considerable reduction of the interparticle space, being in the 0.57-0.98 g/cm^3 range for the H_3PO_4-activated carbons and 0.48–0.81 g/cm^3 for the $ZnCl_2$-activated carbons. On the other hand, the higher the compaction temperature, the higher the bulk density due to the removal of volatile matter during the pressing stage, which favors compaction. Recently, Vargas-Delgadillo et al.[122] and García Blanco et al.,[123] used a similar procedure to prepare activated carbon monoliths from coconut shells with $ZnCl_2$ as activating agent, while Vargas et al. targeted coconut shells and African palm stones using H_3PO_4 as activating agent.[124]

On the other hand, Ramos-Fernández et al.,[125] Wahby et al.[126] and Ruiz et al.[127] took advantage of the self-sintering ability of petroleum mesophase pitch to prepare activated carbon monoliths. Thus, the mesophase pitch was mixed with KOH in a ball-mill, the mixture compacted under uniaxial pressure and finally carbonized. As a result, monoliths with surface area up to 2800 m^2/g and bulk densities in the ~0.15–0.35 g/cm^3 were obtained, which functioned as molecular sieves, being able to discriminate CO_2 (adsorption capacity up to 380 mg CO_2/g sorbent) from molecules of similar dimensions, such as CH_4 and N_2.[126] The monoliths were also used as supercapacitor electrodes, exhibiting high capacitance values in H_2SO_4, i.e. 334 F/g, and very low electrical resistivity, which resulted in a very efficient energy storage device.[127] Similarly, Deraman et al.[128] and Taer et al.[129] took advantage of the self-adhesive properties of pre-carbonized oil palm empty fruit bunches and rubber wood sawdust respectively. The pre-carbonized substances were ball-milled to obtain the self-adhesive grains and then, immersed in H_3PO_4, compressed and carbonized for the oil palm empty fruit bunches, and compressed, carbonized and activated with CO_2 for the rubber wood sawdust. The monoliths prepared from rubber wood sawdust were tested as supercapacitor electrodes, reaching specific capacitance of up to 139 F/g in H_2SO_4.[129]

More recently, Hao et al. synthesized porous carbon monoliths with defined multilength scale pore structures, a nitrogen-containing framework, and high mechanical strength through a self-assembly of poly(benzoxazine-co-resol) and a carbonization process.[130] The N-containing framework was obtained through the use of amines in the synthesis process. Afterwards, the monoliths were subjected to a physical activation step with CO_2 at 900ºC for 1 or 3 h, yielding monoliths with surface area up to 2200 m^2/g. Such monoliths showed encouraging CO_2 capture (~2.6-3.3 mmol/g at 25 ºC) and separation capacities, high selectivity, and facile regeneration at room temperature.

3. Use of activated carbons in energy related applications

3.1 Supercapacitors

Electrochemical double-layer capacitors (EDLCs) rely on charge separation at electrode/electrolyte interfaces to store energy (Figure 6a). The reduction of the charge separation distance to dimensions similar to those of the ions within the electrolyte, i.e. to few nanometers, coupled with the large surface area of the porous electrodes, makes them capable of storing much larger amounts of energy (typically 3-5 Wh/kg) than conventional capacitors. On the other hand, the electrostatic nature of the storing process gives rise to higher power densities, excellent reversibility and longer cycle life compared to batteries. Another kind of electrochemical capacitors or supercapacitors are those referred to as pseudocapacitors, where energy is stored through fast and reversible Faradaic charge transfer reactions between the electrolyte and electroactive species on the electrode surface. Reactions that result in Faradaic charge transfer are mainly of the redox type where changes in the oxidation state of the materials occur, which is analogous to battery systems. The amount of energy stored is higher than in EDLCs (i.e.,

5-30 Wh/kg), although their cyclability and power density is normally lower. Owing to those energy-power characteristics of supercapacitors, they occupy the niche between conventional capacitors and batteries, as clearly seen in the Ragone plot (specific power *vs.* specific energy) depicted in Figure 6b, being ideal devices for short-term power applications, such as uninterruptible power supply systems (back-up supplies to protect against power disruption), regenerating storage, load-leveling, quick charge applications or start-ups.

The use of high capacitance materials (high surface area or highly electroactive species) is a key factor to ensure high energy density in such devices. Nowadays research efforts are focused on the design of electrode materials with tailored PSD, as well as tailor-made electrolytes, to increase the energy density of such devices without compromising their power capability. The incorporation of electroactive species into carbon electrodes is also receiving increasing attention as a way of further increasing the energy stored in such devices.

3.1.1 Electrical double layer capacitors (EDLCs)

Activated carbon is the material used in commercial EDLCs due to its high surface area (> 1000 m^2/g), relatively low cost, adequate electrical conductivity, chemical stability and availability. In 1957 Becker patented the first capacitor based on a high surface area carbon in partnership with the General Electric Company[131] and since then, different companies have undertaken the commercialization of activated carbon-based supercapacitors such as Maxwell Technologies, NESSCAP, NEC, Panasonic or AVX (Figure 7). Most of their commercial supercapacitors are based on powder activated carbon made from coconut shell. Some companies have also built higher performance devices, at a significant cost increase, based on synthetic carbon precursors that are activated with potassium hydroxide (KOH). Some commercially available activated

carbons are commonly used in research for comparison purposes, for example, carbon YP-50F(YP-17) by Kuraray Chemical Co, which is a powdered-type activated carbon produced from coconut shell, and characterized by surface area of 1600-1700 m^2/g and relatively narrow PSD in the micropore range.[132] Other commercially available activated carbons commonly used in research include those manufactured by NORIT, i.e. DLC Super and Supra (~ 1800 and ~ 2100 m^2/g respectively), both of which are steam activated carbons derived from biomass.

Research work devoted to the use and improvement of the performance of activated carbon in EDLCs is extensive. More than 25 years ago, commercial activated carbon fiber cloth was used to build an experimental supercapacitor cell working with organic electrolyte.[133] A specific capacitance of 36.5 F/g was estimated for a material possessing a surface area of 1500-2500 m^2/g (see Table 1). All the reported capacitance values in this review are for a two-electrode cell system unless otherwise stated. Nowadays many works related to the use of activated carbon fibers in supercapacitors working with aqueous or organic electrolytes can be found in the literature.[134,135,136,137,138,139] To date, a variety of carbon materials have been used to fabricate supercapacitor electrodes (i.e. mesoporous templated carbons, zeolite templated carbons, carbon xerogels, carbon nanotubes or carbide derived carbons), but activated carbons are still the primary choice.

Many efforts have been made to correlate the nanoporous structure of activated carbons with their capacitance performance in different electrolytes. So far, no clear linear relationship has been found between specific capacitance and surface area, which may be explained by the inaccessibility of the smallest pores to the solvated ions, different electroadsorption behavior of micropores and the external surface area or pseudocapacitance effects due to the presence of oxygen groups. Thus, Shi studied the

electrochemical performance of 11 activated carbon microbeads and 23 activated carbon fibers in KOH aqueous solution (Table 1).[140] They did not find a linear correlation between the total surface area and the specific capacitance but an apparent dependence on micropore surface area and external surface area. On the basis of their proposed model, the double layer capacitance per unit of micropore surface area was found to be very close to that of carbon basal plane (about 15-20 $\mu F/cm^2$) and the double layer capacitance per unit of external surface area was strongly dependent on the porous structure and surface morphology. Later on, Qu and Shi studied the electrochemical behavior of activated carbons with different surface areas and PSDs in aqueous KOH and found that the bigger the pore, the easier and faster it is accessed electrochemically.[141] On the other hand, Endo et al. analyzed the supercapacitor performance of activated milled mesophase carbon fibers and powder-type activated carbons in organic electrolyte[142] and found a higher specific capacitance for the activated carbon fibers (41 *vs.* 32 F/g, Table 1) in spite of a smaller specific surface area (771 *vs*. 1848 m^2/g), which they attributed to the relative accessibility of the electrolyte ions to the pore structure of the various materials. More recently, Centeno and Stoeckli studied the electrochemical performance of 30 activated carbons in H_2SO_4 (Table 1) and established a two-contributions dependence of the specific capacitance on the total surface area and the concentration of CO-generating surface species.[143] Nowadays, it is known that the ion salvation shell becomes highly distorted and is partially removed in subnanometer pores, giving rise to an anomalous increase in the capacitance in carbon materials with pore sizes less than 1 nm.[35,144] This shows how important it is to match the pore size of the electrode material to the specific electrolyte (aqueous, organic or ionic liquids) and that not only high surface areas are needed, but narrow and controlled PSDs. Recent works on the development of activated carbons for supercapacitor

applications are thus focused on the control of the PSD and pore structure.

As previously mentioned, KOH activation allows control over the PSD of activated carbons. Thus, Raymundo-Piñero et al. prepared a series of activated carbons with progressively changing nanotextural characteristics by heat-treatment of a bituminous coal at temperatures in the range 520-1000ºC, and subsequent activation by KOH at 700 or 800ºC.[145] The surface area of the activated carbons varied from 800 to 3000 m^2/g and the average micropore width between 0.65 and 1.51 nm depending on the carbonization temperature. The specific capacitance of the carbons was analyzed in H_2SO_4, KOH and $TEABF_4$/Acetonitrile solutions, measuring values of ~160–310 F/g, 124-286 F/g and ~120–180 F/g respectively. The higher the surface area, the higher was the specific capacitance, although the specific capacitance per surface area increased at lower pore size, reaching a maximum at ca. 0.7 nm in aqueous media and 0.8 nm in organic electrolyte. Furthermore, saturation of gravimetric capacitance was observed in all electrolytes for the high surface area carbons due to increase of the average pore width. Although the pore volume of these carbons is very high, their pores are too wide for an efficient participation in the formation of the double layer. More recently, Sevilla et al. tuned the porosity of activated carbons prepared from hydrothermally carbonized substances[61] and polypyrrole[40] by the control of the activation temperature (600-900ºC) and the KOH/precursor weight ratio (2 and 4) (see Figure 1d). All the materials were characterized by large surface area and pore volume, in the 2000-3500 m^2/g and 1-2.6 cm^3/g range, respectively. Furthermore, depending on the precursor used, an additional tailoring of the porosity was possible. Thus, whereas the activation of hydrothermally carbonized substances lead to essentially microporous materials, the activation of polypyrrole gave rise to bimodal activated carbon exhibiting one pore size system in the micropore range (1.2-1.3 nm) and another in the mesopore range (2-3.4 nm). The

activated carbons prepared from hydrothermally carbonized substances (HTC-based ACs) were analyzed as electrodes in supercapacitors working with organic electrolyte ($TEABF_4$/AN, AN = acetonitrile), achieving values as high as 236 F/g (100 F/cm^3) (Table 1).[98] This capacitance value is the second highest ever recorded in this kind of electrolyte, after the one reported by Li et al. for KOH-activated straw in $MeEt_3NBF_4$/AN (251 F/g).[146] Furthermore, charge-discharge tests showed excellent capacitance retention with capacitance of up to 175 F/g at a current density of 20 A/g. Additionally, compared to conventionally activated carbons used in commercial devices, such as YP-17D, the HTC-derived activated carbons offer ~100% enhancement in the achieved specific capacitance, which will double the energy density of supercapacitors. On the other hand, the polypyrrole-based activated carbons, with larger pore sizes than the HCT-derived analogues, were analyzed in an electrolyte with larger ions, i.e. an ionic liquid electrolyte ($EMImBF_4$), yielding outstanding results.[147] Thus, they exhibited specific capacitance of up to 300 F/g (Table 1), which is unprecedented for carbon materials and more than a two-fold improvement compared to commercial activated carbons like YP-17D, and 5-8% performance improvement after 10000 charge-discharge cycles at a high current density of 10 A/g.

Kierzek et al. have also prepared KOH-activated carbons with a superior performance in H_2SO_4 electrolyte.[148] They activated various coal and pitch-derived carbonaceous materials at 800ºC for 5 h using a KOH/precursor weight ratio = 4. The produced activated carbons were essentially microporous and exhibited surface area in the 1900-3200 m^2/g range and pore volume of 1.05 to 1.61 cm^3/g. Capacitance values ranging from 200 to 320 F/g were measured, compared to 240 F/g for the commercially available activated carbon, PX-21 (Table 1). Several other studies have reported on KOH-activated carbons with outstanding performance (>250 F/g) in aqueous

electrolytes (Table 1).[127,149,150,151,152,153] There are also studies on KOH activated carbon-based electrodes with modest capacitance values (100 – 200 F/g) in aqueous electrolytes.[154,155,156] For organic electrolyte, the capacitance values are normally lower than 150 F/g.[155,157,158,159,160]

Activated carbons with remarkable performance as supercapacitor electrodes have also been prepared using other chemical agents or physical activation. Thus, Zhang et al. prepared activated carbons by NaOH activation of anthracite with surface area up to ~2500 m^2/g and capacitance values up to 167 F/g in organic electrolyte (Table 1).[161] Interestingly, ion sieving effect was observed for the activated carbon with the smallest pore size. Similarly, Xu et al. prepared activated carbons with surface areas in the 1829-2675 m^2/g range and capacitance values ranging from 108 to 155 F/g in organic electrolyte (Et_4NBF_4/PC, PC = propylene carbonate) (Table 1) by NaOH activation of PVDC.[162] They observed a better rate performance, i.e. better charge propagation, for the materials with larger pore size (see Figure 8), as found also by Wei et al.[98] On the other hand, Rufford et al. have measured specific capacitance up to 300 F/g in H_2SO_4 for $ZnCl_2$-activated sugar cane bagasse and up to 134 F/g in $TEABF_4$/acetonitrile for $ZnCl_2$-activated waste coffee (Table 1).[163,164] Very recently, Wei and Yushin achieved remarkable capacitance values up to 172 F/g in ionic liquid electrolytes ($EMImBF_4$ and $EdMPNTf_2N$) using activated carbons obtained by CO_2-activation of pyrolyzed sucrose (Table 1).[165]

As mentioned in section 2.2, physical or chemical activation processes have been applied to advanced carbon materials such as CDCs, templated porous carbons, carbon aerogels, graphene or nanotubes with the aim of improving their supercapacitor performance. Thus, KOH activation of Ti-CDCs resulted in a 30% increase in specific capacitance compared to the pristine CDC, and reached values as high as 180 F/g in

organic electrolyte (NEt_4BF_4/AN) (Table 1).[102] It was observed that, although subnanometre pores were best suited for improving the capacitance (as probed by higher normalized capacitances, F/m^2), the overall increase in surface area and volume of pores between 1 and 2 nm compensated for the decrease in subnanometre pore volume in the activated CDCs.

Carbon aerogels have been analyzed as supercapacitor electrodes due to their high electrical conductivity, relatively high surface area, controllable pore structure and the possibility of forming monoliths (i.e. increased volumetric capacitance). However, they are predominantly mesoporous, so that a post-synthesis activation step has been applied by several authors to introduce microporosity. Thus, Fang et al. activated carbon aerogels obtained from resorcinol-formaldehyde under a CO_2 flow,[166] which resulted in a doubling of surface area and increase in micropore volume from 0.02 to 0.61 cm^3/g. As a result, the specific capacitance was also doubled up to 100 F/g in Et_4NBF_4/PC. Zhu et al. have also applied a CO_2-activation step to carbon aerogels synthesized from cresol-formaldehyde, increasing the surface area from 245 m^2/g to between 401-1418 m^2/g depending on the activation conditions (temperature and time).[167] This enhancement in porosity was reflected in an increase of capacitance from 78 F/g to up to 146 F/g in KOH electrolyte. Additionally, the activated carbon aerogel showed a good rate performance, only a 10% capacitance decrease being registered with the increase of the current density from 1 to 20 mA/cm^2.

Other types of porous carbons which have been activated with the aim of increasing their microporosity and surface area are templated mesoporous carbons. Zhao et al. performed $ZnCl_2$ activation of a mesoporous carbon, which resulted in a 33% increase in surface area, enhancing thereby the specific capacitance in a Et_4NBF_4/PC solution from 60 F/g for the templated mesoporous carbon to ~ 94 F/g for the activated

carbon (Table 1). [168] Several other studies observed similar results for soft-templated carbons (Table 1).[169,170,171,172]

Carbon nanotubes have been intensively studied as supercapacitor electrodes due to their superior electrical properties, which in combination to their readily accessible surface area, yields high specific power. However, their small surface area (generally < 500 m^2/g) renders low energy density, which limits their practical application. Therefore, their activation has been studied as a means of increasing their surface area and specific capacitance (Table 1).[173-175] In this regard, Xu et al. found that the KOH activation enhances the surface area of CNTs and their specific capacitance, but decreases the electrical conductivity and the rate performance in EDLC.[173] They were able to balance the porosity and conductivity by controlling the activation conditions, yielding activated carbon nanotubes with both high capacitance and good rate performance (Table 1).[174,175]

The unique electronic properties of graphene, as well as its theoretical surface area (2620 m^2/g), make it an attractive material for supercapacitor applications. Since its isolation in 2004, articles devoted to the study of graphene as supercapacitor electrode are increasing. However, the surface area of graphene is normally much lower than the theoretical value (normally < 500 m^2/g) due to agglomeration of graphene sheets, so that the capacitance values achieved are lower than expected (< 200 F/g in aqueous electrolyte, < 120 F/g for organic electrolyte and < 80 F/g in ionic liquids). A possible way to overcome such drawback is its post-synthesis activation. The first to report on the activation of graphene as a tool to enhance its supercapacitor performance was the group of Ruoff.[176] They used KOH to activate microwave exfoliated graphene oxide (MEGO) and thermally exfoliated GO (TEGO), yielding porous materials with surface area and pore volume up to 3100 m^2/g and 2.14 cm^3/g respectively. The activation led to

a continuous 3D network of pores ranging from ~ 0.6 to 10 nm and the suppression of oxygen-containing groups present in the as-synthesized GO. That material exhibited a specific capacitance of 166 F/g in $BMIMBF_4$/AN electrolyte and 150 F/g in $TEABF_4$/AN. The authors estimated the specific energy for a packaged supercapacitor device (based on a weight ratio of 30% for the active electrode material) of above 20 Wh/kg, which is four times higher than existing AC-based supercapacitors; and the power density of ~ 75 kW/kg, which is one order of magnitude higher than the values from most commercial carbon supercapacitors that have energy density values of 4 to 5 Wh/kg. After that pioneering work, many authors have explored the activation (mostly chemical activation with KOH) of graphene[177,178,179,180,181,182] or N-doped graphene[183] for supercapacitors, getting capacitances up to 270 F/g in aqueous electrolyte, ~ 200 F/g in organic electrolyte and ~ 170 F/g in ionic liquid electrolyte, coupled to excellent rate capability (see Table 1).

3.1.2 Pseudo-capacitors

3.1.2.1. Pseudocapacitance caused by heteroatoms

Many activated carbons contain oxygen-containing surface functionalities, which give rise to pseudocapacitance effects (mainly in aqueous electrolytes) that lead to increased specific capacitance and amount of energy stored in the supercapacitor. Thus, with the presence of carbonyl- or quinone-type groups (CO-desorbing groups in TPD experiments), the following equilibrium reaction may occur in the carbon electrode:

$$>C_xO+H^+ = >C_xO//H^+$$

Where $>C_xO//H^+$ represents a proton adsorbed by a carbonyl or quinone-type site induced by ion-dipole attraction. This specific adsorption process may facilitate an excess specific double layer capacitance due to the local changes of electronic charge density. Additionally, during charging of the negative electrode, a strong bond may

form between carbonyl- or quinone-type groups and protons due to electron transfer across the double layer:

$>C_xO+H^++e^- = >C_xOH$

The backward reaction would proceed during discharge. This redox reaction gives rise to a pseudocapacitance component of the overall capacitance of the material.[184] It is reflected in cathodic and anodic humps in CV experiments at around 0.5-0.6 V vs. RHE.[185] Furthermore, oxygen functional groups that are electrochemically inert can improve the wettability of the carbon electrode and, consequently, enhance the specific capacitance through improved pore access and greater surface utilization.[186] On the other hand, high-polarity oxygen groups such as carboxyl, anhydride and lactone (CO_2-desorbing groups), may hinder the motion of ionic species, increasing the resistance and causing capacitance fading at high current density.[184,187] In this regard, Centeno and Stoeckli have correlated the specific capacitance at low current density of activated carbons with the amount of CO-desorbing groups and the total surface area, whereas the evolution of the specific capacitance with the increase of the current density was correlated to the amount of CO_2-desorbing groups and the average pore width, L_0.[96] Bleda-Martínez et al. found also a good correlation between the specific capacitance of activated carbons and the amount of surface oxygen groups desorbing as CO.[48] Many other reports on pseudocapacitance contribution of oxygen-groups in activated carbons are available.[188,189,190,191,192,193,194]

Oxidation treatments, both chemical (HNO_3 or H_2SO_4) and electrochemical, have also been applied to activated carbons to generate oxygen-containing functionalities, increasing the specific capacitance of the material.[195,196,197,198,199] Additionally, Mysyk et al. have shown that a high concentration of oxygenated surface functionalities can prevent further oxidation of the activated carbon, allowing operation

in a wider potential window.[197]

Another heteroatom which is known to give rise to Faradaic pseudocapacitive reactions in carbon materials is nitrogen. It can be present in the activated carbon due to the use of a N-rich carbon precursor (e.g polypyrrole,[40] polyacrylonitrile[200] or waste coffees[189]) or through the modification of the activated carbon surface by introduction of nitrogen containing groups, using melamine[192, 201] or urea[192,201] followed by heat-treatment, or by thermal treatment with ammonia[202 , 203 , 204] or ammoxidation (i.e. air/ammonia mixture).[205 , 206] The nature of the nitrogen-containing surface differs depending on the temperature of heat treatment. It is believed that amides, aromatic amines and protonated amides (functional groups external to the aromatic ring structure) are predominant at low temperature (400–700 ºC) while pyridine, pyrrole, aromatic amines, quaternary nitrogen and protonated pyridine (nitrogen within the aromatic ring structure with a delocalized charge or no charge) dominate at higher temperature (> 700ºC).[203,207] Seredych et al. found a strong dependence of capacitance on the chemistry of N-containing surface groups, as well as the porosity, for activated carbons oxidized and then treated with melamine and urea followed by carbonization at 950ºC in an inert atmosphere.[201] Their results showed a direct relationship between the number of basic groups determined from wet titration and the gravimetric capacitance, particularly at high current densities, and between the normalized capacitance per volume of micropores and the population of quaternary nitrogen and pyridine-N-oxide inside the pores. The conclusion was that pseudocapacitive interactions take place on negatively charged pyrrolic-N and pyridinic-N, while the positive charge on quaternary-N and pyridine-N-oxide helped in electron transport through the carbon. In this way, N-doped activated carbons exhibited specific capacitances of 260 and 330 F/g in H_2SO_4 for melamine- and urea-treated activated carbons respectively (Table 1). It was observed

that although the quaternary and pyridinic-N-oxides nitrogen groups had enhancing effects on the capacitance due to the positive charge and thus improved electron transfer at high current densities, the most important functional groups affecting energy storage performance were pyrrolic and pyridinic nitrogen, along with quinone oxygen.[192] Experimental data for supercapacitors prepared with N-doped activated carbons are indicated in Table 1. [189,192,200,201,205, 206,208,209]

Pseudocapacitance caused by sulphur-containing groups in activated carbons, such as sulfone, sulphide or sulfonic groups, is just starting to be analyzed, with only one report having been published to date. Hasegawa et al. have observed humps in CV experiments at around -0.2 to 0 V *vs.* Hg/Hg_2SO_4 for a monolithic S-containing activated carbon, which they attribute to the oxidation-reduction of sulfur-containing groups such as sulfo groups.[210] The S-doped activated carbon, with a surface area of 2420 m^2/g and a S/C = 0.83% in atomic percentage, exhibited a specific capacitance of 205 F/g in H_2SO_4 electrolyte (Table 1).

3.1.2.2. Pseudocapacitance in composites AC/metal oxide or AC/conducting polymer

Another possibility for the introduction of a pseudocapacitance contribution in supercapacitors prepared with activated carbons is via the synthesis of composites comprising activated carbon and electroactive species such as metal oxides (Ru_2O, NiO, MnO_2, Fe_3O_4…) or conducting polymers (polyaniline, polypyrrole, polythiophene and their derivatives). In the case of metal oxides, the activated carbon matrix provides the metal oxide, normally of poor electrical conductivity, with an excellent media for electron conduction, improving its rate performance. For composites based on conducting polymers, the carbon matrix can buffer the volume changes suffered by the polymer during charge/discharge processes, thus improving the cycling performance.

Among the various metal oxides, ruthenium shows the best pseudocapacitive behaviour. However, it has the major drawback of being costly, which has limited its use. One way to reduce cost is to minimize the amount of Ru used by dispersing it over high surface area materials, such as activated carbons. In this regard, Sato et al. reported a 20% increase in specific capacitance by loading 7.1 wt% Ru in activated carbon.[211] Ramani et al. deposited varying loads of RuO_2 on activated carbon through an electroless deposition process and observed that at higher RuO_2 loading, an enhancement of the specific capacitance (measured in the three-electrode cell configuration) took place from 145 F/g for the 5 wt% composite to 260 F/g for 20 wt% RuO_2 loading, whereas the bare carbon had a specific capacitance of 98 F/g (Table 2).[212] Similarly, Zhang et al. prepared amorphous hydrous ruthenium oxide/active carbon ($RuO_2 \cdot xH_2O$/AC) powders and observed that the specific capacitance was proportional to the mass of the ruthenium in the electrodes.[213] For 10-20 wt% of ruthenium in the electrodes, the specific capacitance remained almost unchanged at 243 F/g, whereas from 35 wt% to pure $RuO_2 \cdot xH_2O$, the specific capacitance increased from 350 to 715 F/g (Table 2). There are other examples where enhancement of specific capacitance is observed when ruthenium oxide is added to activated carbons despite a reduction of surface area of the composite (Table 2).[214,215,216,217,218,219]

Manganese oxides are considered as one of the most promising transition metal oxides for next generation supercapacitors due to their low cost non-polluting nature, ideal capacitor performance and high safety during operation. Despite the theoretical expectation that electrodes made from manganese oxide should exhibit high specific capacitance and rate capability, their poor cycling stability and rate capability arising from low conductivity have limited their performance in practical applications. One strategy to overcome these limitations is the formation of composites with conducting

materials, such as graphene, carbon nanotubes or activated carbon. Thus, very recently Lee et al. doped a KOH-activated carbon aerogel with 7 wt% of manganese oxide (γ-Mn_3O_4) by an incipient wetness impregnation method, achieving a specific capacitance of 168 F/g (three-electrode cell system) in KOH electrolyte, whereas the specific capacitance of the activated carbon aerogel with surface area of 1447 m^2/g was 136 F/g (Table 2).[220] Li et al. have reported a specific capacitance of 183 F/g in 1 M $LiPF_6$ (EC + DMC) organic electrolyte at operating voltage up to 3.0 V for MnO_2 nanostructures (short fiber-like structures) coated onto activated mesocarbon microbeads (MCMB).[221] The specific capacitance based on the MnO_2 was estimated to be as high as 475 F/g, corresponding to a considerable energy density of 106 Wh/kg. A composite consisting of activated mesocarbon microbeads and Mn_3O_4 with specific capacitance of 178 F/g in 1 M $LiPF_6$ (EC + DMC) has been reported by Wang et al.[222] Malak-Polaczyk et al. have prepared composites of commercial activated carbons and λ-MnO_2,[223] and showed that introducing λ-MnO_2 into the activated carbons enhanced effective utilization of λ-MnO_2; a synergetic effect of the porous carbon framework and the redox properties of λ-MnO_2 was at the origin of improvement of specific capacitance values in comparison with the activated carbons. Other composites between activated carbon and manganese oxides have been reported (Table 2).[224,225] On the other hand, Selvakumar et al. have prepared composites by physical mixing of ZnO and commercial activated carbon and achieved capacitances of 42-76 F/g (three-electrode cell system) at 50 mV/s in Na_2SO_4 for ratios AC:ZnO = 1:3–1:1. The specific capacitance of the electrodes decreased with increase in zinc oxide content.[226]

Nickel oxide/hydroxide is another electroactive species commonly used in pseudocapacitors. Huang et al. prepared a nickel hydroxide/activated carbon composite by a simple chemical precipitation method, which exhibited specific capacitance of

292–314 F/g for a $Ni(OH)_2$ content of 2 to 6 %, which was 23.3% higher than pure activated carbon (255 F/g). For larger contents of $Ni(OH)_2$, 8–10%, a decrease of the capacitance was registered, being in the range 261-302 F/g (three-electrode cell system). Additionally, the composite electrodes had good electrochemical performance and high charge–discharge properties.[227] Another transition metal oxide which has been added to activated carbons and found to increase specific capacitance is TiO_2.[228,229,230]

Regarding the preparation of activated carbon/conducting polymer composites, polyaniline (PANI) has drawn the most attention due to its high conductivity and stability, and low cost. Thus, Ling and Teng electrodeposited PANI onto microporous activated carbon fabric, recording specific capacitances up to ~320 F/g in H_2SO_4 (three-electrode cell system).[231] Similarly, Wang et al. polymerized aniline using cyclic voltammetry onto activated carbons.[232] The PANI/AC composite electrodes had better cycling stability than PANI electrodes and the specific capacitance of the composite electrodes was 587 F/g (three-electrode cell system), which was much higher than that of the pristine activated carbon (140 F/g), owing to the faradic reaction of PANI with the electrolyte. Furthermore, the PANI electrode was less stable than the PANI/AC composite electrode with a capacitance decay of ~35% for the former and 7% for the latter after 50 cycles. Bleda-Martínez et al. prepared PANI/AC composite electrodes via two different methods: i) mechanical mixing of the activated carbon and chemically polymerized PANI, which yielded electrodes with specific capacitance of 273-316 F/g (three-electrode cell system) in H_2SO_4 electrolyte, and ii) chemical polymerisation of aniline loaded in activated carbon, which led to electrodes with specific capacitance of 125-187 F/g (three-electrode cell system).[233] It was shown that the method used for the preparation of the composites strongly affects the porous structure. With regards to electrochemical performance, polyaniline and carbon mechanically mixed seem to work

independently, with the composite behaviour being a combination of the corresponding performance of the constituents separately. On the other hand, the composites prepared by polymerisation over carbon revealed that the polyaniline coating strongly depends on surface chemistry; aniline reacts with the oxygen complexes, eliminating their positive effect on capacitance and producing important changes in porosity. Further capacitance data for AC/PANI composites are given in Table 2.[234,235,236]

3.1.3. Hybrid supercapacitors

The quest for higher energy densities able to fulfil the ever-increasing energy demand of the society and latest generation of technology has spurred the development of hybrid supercapacitors, regarded as the second generation of supercapacitors. Hybrid supercapacitors are those where the positive and negative electrodes are made of different materials, one of them being always an EDLC-type electrode (i.e. carbon material). Depending on the nature of the materials used, there are two types of hybrid supercapacitors, i.e. asymmetrical supercapacitors (EDLC-type electrode+pseudocapacitance-type electrode) and lithium-ion capacitors (or battery-like capacitors, EDLC-type electrode+battery-type electrode), which are described in detail below. It is worth noting that in both kinds of devices, activated carbons are the unanimous choice as EDLC-type electrode. It is also worth mentioning that normally commercial activated carbons are used. The use of tailor-made activated carbons may improve the performance of these devices to a further extent. It should be noted that taking into account the large disparity in performance characteristics between the two electrodes, mass balancing of the two electrodes is critical to ensure the most efficient utilization of each electrode and optimal cycle life.[237]

3.1.3.1 Asymmetrical supercapacitors

Asymmetrical capacitors are those comprised of an EDLC-type electrode (carbon material) and a pseudocapacitance-type electrode (metal oxides/nitrides, conductive polymers or a composite carbon/pseudocapacitive material). Asymmetrical capacitors, therefore, combine the energy characteristics of pseudocapacitive materials (fast redox reversible reactions) with the power and cycling characteristics of carbon materials (ultra-fast electrostatic ion adsorption and robust cycle life), overcoming thereby the limitations of both constituent materials. In most cases, the negative electrode is composed of an activated carbon, whereas the positive electrode comprises the pseudocapacitive material. This particular configuration allows a substantial enlargement of the working voltage window when working with aqueous electrolytes (sometimes well beyond the thermodynamic limit of 1.2 V) as a result of the high overpotentials for H_2 and O_2 evolution at the carbon-based negative electrode and the pseudocapacitance-type positive electrode, respectively. This enhances the energy density of the device even more. For example, the operational voltage of AC/nanostructured CoAl double hydroxide can reach 1.5 V in KOH (energy density = 15.5 Wh/kg, power density = ~ 0.3 kW/kg, and 90% of initial capacity kept over 1000 cycles) (see Figure 9a),[238] that of AC//α-$Ni(OH)_2$ is 1.6 V in KOH,[239] and that of AC//manganese oxide is up to 2.0-2.2 V in KNO_3, Li_2SO_4 or Na_2SO_4 (see Figure 9b).[240,241,242] Likewise, AC nanofibers//graphene-MnO_2 supercapacitor works up to 1.8 V in Na_2SO_4, exhibiting a maximum energy density of 51.1 Wh/kg (at a power density of 0.1 kW/kg) and excellent cycling durability, with 97% of the specific capacitance retained after 1000 cycles.[243]

In the case of asymmetric capacitors consisting of AC//conducting polymers, enhanced cyclic stability is obtained compared to symmetric capacitors prepared with

conducting polymers only. Thus, Fabio et al. successfully cycled an AC//p-doped poly(3-methylthiophene) supercapacitor over 10000 cycles in organic electrolyte at 20 mA/cm^2 with 1.0–3.0 V cut off potentials.[244] Likewise, Laforgue et al. fabricated a prototype of AC//poly(4-fluorophenyl-3-thiophene), which withstood 8000 cycles over the voltage range 1.0-3.0 V in organic electrolyte. Half of the capacitance was lost during the first 100 cycles, but then it remained constant (providing an energy density of 3.3 Wh/kg) for the rest of the cycling test.[245] Laforgue et al. also developed 3V and 1.5 kF supercapacitor modules, and 2 kW stacks based on hybrid cells with poly(3-methylthiophene) as positive electrode and activated carbon as the negative electrode in acetonitrile-free organic electrolyte in the framework of an EU project.[246]

3.1.3.2 Lithium-ion capacitors

Lithium-ion capacitors (or battery-type capacitors) are characterized by the combination of a battery-type electrode, such as lithium intercalation compounds, and an EDLC-type electrode, i.e. carbon material (see Figure 10a). Fast charge capability, robust cycle life, and high energy density are likely to be achieved with a Li-ion capacitor. Thus, as Li^+ intercalation-deintercalation in the battery-type electrode occurs in a shallower state-of-charge (SOC) in comparison to a Li-ion battery working with the same electrode, higher cycling stability and safety may be achieved. In this kind of devices, activated carbon is normally used as carbon material and, unlike asymmetrical supercapacitors, it is used as positive or negative electrode equally, depending on the redox potential of the Li-intercalation compound used (see Figure 10b). [237]

Amatucci et al. were the first to report on this novel concept of mixed battery/supercapacitor cell in a series of papers. The first one was related to the preparation of a cell with activated carbon as positive electrode and nanostructured $Li_4Ti_5O_{12}$ as negative electrode, using $LiPF_6$ EC:DMC electrolyte (PF_6^- anions adsorb

on the AC surface, whereas Li^+ cations intercalate into the $Li_xTi_5O_{12}$ lattice).[247] The use of an intercalation compound as the negative electrode offers the opportunity to effectively pin the electrode voltage at potentials very negative with respect to SHE and maintain acceptably high gravimetric and volumetric energy densities as opposed to a pseudocapacitive reaction. The cell exhibited a sloping voltage profile from 3 to 1.5 V (composite voltage profile resulting from the flat two-phase intercalation voltage profile of $Li_4Ti_5O_{12}$ and the linear voltage profile typical of a carbon EDLC), 90% capacity utilization at 10C charge/discharge rate (6 min.), and 10-15% capacity loss after 5000 cycles. Afterwards, Brouse et al. investigated TiO_2-B as a possible candidate to replace $Li_4Ti_5O_{12}$ as negative electrode, while keeping AC as positive electrode ($LiPF_6$ EC:DMC was also used electrolyte).[248] The cell exhibited energy densities between 45 and 80 Wh/kg with power densities in the 0.2-0.4 kW/kg range, which is compatible with a fast charging/discharging storage device, intermediate between EDLC and Li-ion batteries. The maximum cell voltage could be set between 2.75 and 3.5 V. More recently, Aravindan et al. fabricated a non-aqueous ($LiPF_6$ in EC:DEC) Li-ion capacitor with AC as positive electrode and synthesized sub-micron size $LiCrTiO_4$ particles as anode.[249] The Li-ion capacitor delivered maximum energy and power densities respectively of 24 Wh/kg and 4 kW/kg, and exhibited as well enhanced capacitive retention properties. On the other hand, Kim et al. analysed non-aqueous ($LiBF_4$+$TEABF_4$ in AN) cells comprising AC as negative electrode and composites of AC and Li transition metal oxides, such as lithium cobalt oxide ($LiCoO_2$) and lithium manganese oxide ($LiMn_2O_4$), as positive electrodes.[250] The specific capacitance and energy density of the cell improved as the content of the Li transition metal oxide increased in the composite positive electrode, showing 60% increase compared to those of a symmetric supercapacitor prepared with the AC. Similarly, Mladenov et al.

fabricated a non-aqueous ($LiPF_6$ in EC:DMC) cell composed by activated graphitized carbon as negative electrode and AC/$Li_4Ti_5O_{12}$ composite as positive electrode.[251] Symmetric cells were also constructed with the AC for comparison, registering an increase of 100% in capacitance for the asymmetric cell. The cycling stability was relatively good (up to 600 cycles).

Unlike Li-ion batteries, Li-ion capacitors may also be fabricated with aqueous electrolytes, which simplifies the fabrication and packaging process (no need for a glove box or dry room). For example, Wang and Xia prepared a cell with AC as negative electrode and $LiMn_2O_4$ as positive electrode in a mild Li_2SO_4 aqueous electrolyte.[252] The charge/discharge processes are only associated with the shuttle of Li ions between the two electrodes, as in a conventional Li-ion battery. Therefore, the electrolyte mainly functions as an ionic conductor and is not consumed during the charge/discharge processes. This overcomes the drawback of electrolyte depletion during the charge process of conventional Li-ion capacitors, a problem studied in detail by Zheng.[253,254,255,256,257] The hybrid cell exhibited a sloping voltage profile from 0.8 to 1.8 V, and delivered an estimated specific energy of ca. 35 W h/kg based on the total weight of the active electrode materials. Furthermore, the cell exhibited excellent cycling performance, with less than 5% capacity loss over 20000 cycles at 10C (0.2 A/g of the total active electrode materials) charge/discharge rate. Very recently, Yan et al. developed an aqueous Li-ion capacitor ($LiNO_3$ electrolyte) with AC negative electrode, but using the widely studied $LiFePO_4$ as positive electrode.[258] They observed that the rate capability of the Li-ion capacitor was much improved compared with that of the battery electrode. Additionally, the stable voltage window was extended up to 1.7 V.

3.2 Hydrogen Storage

The development of porous materials capable of storing enough hydrogen to accomplish the targets required for on-board applications[259,260, 261, 262] still remains a challenge. For this purpose a great variety of highly porous materials such as MOFs,[263,264,265, 266,267, 268] zeolites, [268, 269,270,271] zeolite-like carbon materials[272,273,274,275,276,277,278,279,280] and carbide-derived carbons[281,282,283,284] have been investigated. In particular, carbon-based porous materials have been extensively studied as potential hydrogen stores due to their high surface area, large pore volume, good chemical stability and the ease with which their porosity can be tailored. For example, a hydrogen uptake of 6.9 wt% (at -196ºC and 20 bar) has been reported for templated carbons,[272] while for carbide-derived carbons (CDCs) the typical hydrogen uptake measured is ca. 4.4 wt% (at -196 ºC and 20 bar).[33,34, 281-284] Although templated carbons and carbide-derived carbons are making important and valuable contributions to studies on hydrogen storage, it is the case that activated carbons remain one of the most studied class of carbons as hydrogen stores.

Reports on the use of activated carbons for hydrogen storage started appearing about thirty years ago. In 1980 Carpetis and Peschka[285] reported on the hydrogen storage capacity of several adsorbents, including activated carbons, in the temperature range -208 to -123^{o}C and pressure up to 41.5 bar. They observed a maximum nominal uptake of 5.2 wt% at 41.5 bar and -208^{o}C. The work of Carpetis and Peschka gave an early indication of the potential of activated carbons as hydrogen stores although there was still no clarity on the key parameter involved in the hydrogen adsorption process. The work of Schwarz and co-workers provided some insights on the effect of surface modifications, including acidity and heteroatom (metal) doping, and purity of hydrogen on uptake in activated carbons.[286,287,288,289,290] The maximum storage values observed by Schwarz and co-workers were similar to those reported by Carpetis and Peschka. Based

on the results of a parametric and comparative study of hydrogen adsorption on activated carbon vis-à-vis compressed gas storage as a function of temperature, pressure and adsorbent properties, Chahine and Benard concluded that adsorption on activated carbon can be more efficient than compressed gas but only at cryogenic temperatures. They identified bulk density and surface area as properties that are important in achieving activated carbons with better performance than compressed gases. [291]

3.2.1 Room temperature hydrogen storage

Although much work on hydrogen storage on activated carbons has been performed at cryogenic temperature, there have been many studies on ambient temperature storage. The largely physisorption nature of hydrogen uptake in activated carbons, however, means that uptake at ambient temperature is generally low or very low, and significant storage is only realized at very high pressure. Nevertheless, for operational purposes, it would be most desirable to achieve high amounts of hydrogen storage at room temperature or at near ambient condition. Several studies have explored the hydrogen uptake of activated carbons at near ambient temperatures, typically 25^{o}C. In this regard, Linares-Solano et al,[292] studied the hydrogen storage on a range of activated carbons and activated carbon fibers at ambient temperature and found a maximum uptake at 100 bar of 1 wt% for an activated carbon derived from anthracite. The study concluded that the optimum pore size for hydrogen storage is that which can hold two layers of adsorbed hydrogen (i.e., pore size of about 0.6 nm). Similar conclusions on the optimum pore size of activated carbons for hydrogen storage were arrived at by Vix-Guterl and co-workers. [293] The importance of porosity of activated carbons in determining the hydrogen uptake is illustrated by the study of Jordá-Beneyto[72] wherein hydrogen adsorption measurements were carried out at room temperature and -196^{o}C and high pressure on a series of chemically activated carbons. At room temperature, excess

storage capacity was 1.2 wt% and 2.7 wt% at 200 bar and 500 bar respectively, and the hydrogen uptake was dependent on both the micropore volume and the micropore size distribution. Largely similar results were obtained at ambient temperature by Jin et al. who observed a maximum hydrogen uptake of 0.85 wt% at 100 bar for coconut shell derived activated carbons with a surface area of 2800 m^2/g.[294]

More recently, Gao and co-workers have claimed an apparently much higher hydrogen uptake of 1.46 wt% at a modest pressure of 40 bar for high surface area (3144 m^2/g) activated carbon derived from rayon-based carbon fibers.[295] On the other hand, Fierro et al.[296] reported a maximum excess hydrogen uptake of 0.6 wt% at 25^oC and 50 bar which is similar to the total amount adsorbed on coffee bean-derived activated carbon at 120 bar,[297] while a value of 0.8 wt% was observed by Bhat and co-workers at 20 bar.[298] Sun and Webley observed a maximum hydrogen uptake of 0.44 wt% at 25^oC and 50 bar for activated carbons derived from agricultural waste corncob with surface area and pore volume of up to 3012 m^2/g and 1.7 cm^3/g, respectively, and also determined the parameter representing full coverage of the solid surface of a high surface area activated carbon from the Langmuir–Freundlich equation as being 9.73 mmol/g or 2 wt% at 25^oC.[299]

Apart from petroleum and biomass-derived carbons, other activated carbons from a rich variety of carbon precursors have been investigated as hydrogen stores at room temperature. Examples of such activated carbons include those derived from multi-walled carbon nanotubes, whose hydrogen uptake at 25^oC and pressure of between 3 and 19 bar exhibited linear pressure dependence such that at 19 bar pristine MWNTs stored 0.2 wt% of hydrogen, while activated MWNTs had a slightly higher capacity of 0.32 wt%.[300] The improved hydrogen uptake was attributed to an increase in the micropore contribution from 50% in pristine to 70% in activated MWNTs. A

similarly low uptake of 0.2 wt% at 26°C and 10 bar was obtained for activated carbon nanofibers with a surface area of 570 m^2/g.[301] Polyacrylonitrile (PAN)-based carbon nanofibers (CNFs) prepared by the electrospinning method and heat treatment were activated with KOH and $ZnCl_2$.[302] Although KOH activated CNFs had higher surface area, which increased from 17 to 2420 m^2/g, they only achieved a maximum hydrogen uptake of 1.03 wt% at 30°C and 30 bar. On the other hand, CNFs activated by $ZnCl_2$ achieved a lower surface area of only 744 m^2/g but higher hydrogen uptake of 1.54 wt%, which leads to the conclusion that, even though total surface area and pore volume were important factors for increasing the capacity of hydrogen adsorption, the pore volume associated with pore width (0.6–0.7 nm) was a much more effective factor.[302] Chen and co-workers also investigated KOH activated polyaniline-based carbon tubes of surface area and pore volume up to 2415 m^2/g and 1.55 cm^3/g respectively, and reported a maximum hydrogen uptake of 0.62 wt% at 20°C and 75 bar.[303] Polystyrene based ion exchangeable resins activated with KOH generated activated carbons with hydrogen uptake of 0.81 wt% at 25°C and 100 bar.[304] The presence of micropores was more important in determining hydrogen uptake than total surface area or pore volume. Elsewhere, Ryoo and Choi,[103] activated ordered mesoporous carbons to generate activated carbon with micropore volume and surface area up to 1.0 cm^3/g and 2700 m^2/g, respectively. The hydrogen adsorption capacity of the activated carbons increased approximately linearly with micropore volume and surface area to reach a maximum of 0.75 wt% at 25°C and 100 bar. On the other hand, Gao and co-workers activated a nitrogen-doped ordered mesoporous carbon which achieved surface area of 2498 m^2/g and hydrogen uptake of 0.88 wt% at 25°C and 80 bar.[305]

The ambient temperature hydrogen storage capacity of activated carbons is, to date, limited to a maximum of ca. 1 wt% at moderate pressure (50–100 bar), and ca. 3.0

wt% at very high pressure (i.e., 500 bar). This may be explained by the fact that the isosteric heat of hydrogen adsorption on activated carbons, which is in the range 5–8 kJ/mol, is too low to allow large uptake of molecular hydrogen at room temperature. Although it is clear that there is an optimum pore size for hydrogen adsorption, and that achievement of such a pore size in activated carbons can improve hydrogen storage at room temperature, real breakthroughs may not be possible via modification of textural properties alone. The isosteric heat of hydrogen adsorption has to be higher in order to achieve meaningful storage at room temperature. Isosteric heat of hydrogen adsorption on activated carbons may be increased via surface modifications, including doping with metal atoms or other heteroatoms such as nitrogen or boron, as will be described in the following sub-sections

3.2.1.1 Effect of surface modifications and metal doping

There are very few experimental studies on the effect of the activated carbon surface properties (i.e., functionality), and in particular the presence of oxygen or nitrogen heteroatoms, on hydrogen storage. This is despite several theoretical studies that predict changes in hydrogen uptake of porous carbons due to heteroatom substitution of carbon.[306,307,308,309] Of particular interest is nitrogen-doping, which is theoretically predicted to cause changes in hydrogen uptake of carbons.[310,311] Regarding the effect of surface oxygen on hydrogen storage of activated carbons, Huang and co-workers studied the influence of surface oxides on activated carbon prepared with KOH as activating agent and litchi wood as precursor.[312] The textural properties of the activated carbons significantly reduced while surface acidity increased after oxidation with nitric acid or hydrogen peroxide. The hydrogen storage capacity of oxidized activated carbons, at -196^{o}C and 1 bar, was significantly reduced from 2.6 wt% to below 2 wt% when the acidic group content exceeded 0.8 mmol/g, reducing to as low as 0.7 wt% for an acid

content of 2.1 mmol/g. However, the surface area of the activated carbons also decreases at high acid content, and could contribute to the decreased hydrogen uptake. Zhao and co-workers also studied the effect of oxygen and nitrogen functional groups on the hydrogen uptake of activated carbons and observed a small detrimental effect, which they related to decreased adsorbate-adsorbent and increased adsorbate-adsorbate interactions.[313]

It has been suggested that dispersed metal nanoparticles within a high surface area substrate (such as a porous carbon) can enhance hydrogen storage. It is thought that the resulting metal/porous material composites may take up hydrogen via two processes; (i) adsorption of hydrogen on the surface of the pores of the porous material and (ii) hydrogenation on the metal nanoparticles by forming metal hydrides.[314] The later process (hydrogenation) is due to chemisorption of atomic hydrogen on the metal nanoparticles, which can then initiate a mechanism referred to as hydrogen 'spillover'.[315,316,317,318] Furthermore, Nalm and co-workers have established that hydrogen spillover does not only improve hydrogen capacity but also increases initial hydrogen adsorption kinetics.[319] However, the very existence of a spillover mechanism has been strongly debated with some experimental results reporting findings that revealed very low hydrogen capacities after metal doping.[320,321] The details of spillover as applied in hydrogen storage processes are thus yet to be clearly understood due to the disparity in experimental data. Nevertheless, the spillover of atomic hydrogen is a well-established process in heterogeneous catalysis.[322,323,324,325] More recently, several reports have claimed to show proof of the existence of hydrogen spill-over process on metal-doped activated carbons.[326,327,328,329]

Li and Yang studied the equilibrium and kinetics of hydrogen storage on Pt-doped superactivated carbon (AX-21) containing 5.6 wt% Pt.[330] The Pt was doped via

ultrasound-assisted impregnation of H_2PtCl_6 in a solution of acetone. At room temperature and 100 bar, the hydrogen storage capacity of the Pt-AX-21 sample (surface area of 2518 m^2/g) increased by a factor of 2 to 1.2 wt% compared to ca. 0.6 wt% for the undoped AX-21 (surface area of 2880 m^2/g). The enhancement of hydrogen adsorption was attributed to the dissociation of hydrogen molecules on the Pt surface and the subsequent surface diffusion and adsorption of atomic hydrogen on the carbon surface. In contrast, in a related study by Stadie et al, Pt-doped superactivated carbon (surface area = 2810 m^2/g) had a hydrogen uptake of 0.53 wt% at room temperature and 70 bar, which was lower than the uptake (0.64 wt%) of the unmodified superactivated carbon (surface area = 3420 m^2/g).[320] It was claimed that Pt doping offered no increase in hydrogen uptake and that any hydrogen spillover sorption was below the detection limit of standard volumetric gas adsorption measurements. It was reasoned that due to the additional mass of the Pt and decreased surface area in the platinum doped superactivated carbon, the net effect of spillover sorption was detrimental for gravimetric density of hydrogen. These contrasting results from a similar set of experiments[320,330] illustrate more generally the on-going discussion on the merits of and mechanism of the spillover process as applied to hydrogen storage in metal-doped porous materials at room temperature.

The method of metal doping also plays a role in the level of enhanced hydrogen uptake. Li et al. claimed a threefold increase in hydrogen uptake for Pt-doped activated carbon wherein the Pt was introduced via plasma treatment.[331] The doping of Pt (3 wt%) on activated carbon (of surface area = 1200 m^2/g) was significantly improved by plasma treatment due to increased dispersion and stronger interactions between metal particles and the carbon, both of which, it was claimed, enhanced room temperature hydrogen spillover and storage. The undoped activated carbon had a hydrogen storage capacity of

~0.3 wt% at room temperature and 100 bar, which was enhanced to ~0.5 wt% by doping with 3 wt% Pt via H_2 reduction, and up to ~0.9 wt% when doping was via plasma treatment.

Despite the lack of clarity on the hydrogen spillover process, there is now general agreement that metal doping can increase the hydrogen uptake of carbons under certain conditions. The extent of the increase in hydrogen storage is dependent on the measurement conditions (temperature and pressure) and the balance between metal loading, metal dispersion and changes in textural properties (surface are and pore volume) after metal doping. To date, the available data on hydrogen storage on metal-doped activated carbons shows reasonable consistency. Metal-doped activated carbons have therefore proved quite attractive as hydrogen stores compared to other types of metal doped carbon forms (e.g., nanotubes, nanofibers).

A variety of other transition metals have been explored including Ni,[332,333,334] Pd,[335,336,337] Vd,[338] and Co.[339] Zielinski and co-workers studied hydrogen storage at room temperature on a commercial activated carbon impregnated with Ni. [332,333] In the absence of metal, the activated carbon, with surface area of 1073 m^2/g and pore volume of 0.6 cm^3/g, stored a maximum of ca. 0.15 wt% of hydrogen at 30 bar. On the other hand the metal-doped activated carbon containing 1 wt% Ni could store up to 0.53 wt% hydrogen at 30 bar. The increase in hydrogen storage was attributed to the hydrogen stored being loosely chemisorbed in the form of spilt-over species through dissociation of molecular H_2 on the Ni and migration onto the activated carbon surface. Recently, Yang et al. claimed a threefold increase in room temperature hydrogen storage in Ni-doped activated carbon.[334] The Ni-doped activated carbon achieved a maximum storage capacity of 0.79 wt% at 300 bar. A small Ni particle size was a critical factor that determined the enhancement of room temperature hydrogen storage.

In a study by Anson and co-workers, Pd-doped activated carbon (MAXSORB) was found to have enhanced ambient temperature hydrogen uptake capacity at low (1 bar) and intermediate (90 bar) pressure.[335] At 1 bar, the capacity of Pd-MAXSORB was more than 1 order of magnitude greater than the 0.01 wt% for undoped MAXSORB and reached 0.3 wt% and 0.5 wt% at Pd loading of 30 and 50 wt% respectively. However, at 90 bar, undoped MAXSORB stored 0.42 wt% hydrogen compared to 0.4 wt% and 0.7 wt% at Pd loading of 30 and 50 wt%, respectively, meaning that the increase in the hydrogen capacity after doping decreased at high pressure. It should be noted that the surface area of the MAXSORB decreased significantly from 2100 m^2/g to 500 m^2/g and 200 m^2/g at Pd loading of 30 and 50 wt%, respectively. Elsewhere, it has been noted that the amount of hydrogen stored at room temperature in Pd-doped activated carbons increases with Pd content as long as the amount of metal stays below ca. 10 wt%. [336,337] In a study by Im and co-workers, vanadium embedded activated electrospun carbon fibers with high surface area of 2780 m^2/g were found to have a high hydrogen storage capacity of ca. 2.5 wt% at room temperature and 100 bar.[338]

There have also been attempts to enhance the hydrogen uptake of activated carbons via metal doping in the presence of metal organic frameworks. In this case, the claim is that bridges are formed between the various components to engender transfer of spillover hydrogen and greater hydrogen storage. Lee and co-workers doped Pt onto activated carbons (AC)/metal-organic framework (MOF-5) composites. [340] It was claimed that the hydrogen storage capacity of the Pt-ACs-MOF-5 composites was 2.3 wt% at room temperature and 100 bar, which was an enhancement factor of five times and three times compared with raw ACs and MOF-5, respectively.

3.2.2 Cryogenic hydrogen storage

Analysis of existing data on room temperature hydrogen storage indicates that, at the moment, only small amounts (maximum of ca. 3 wt%) can be stored in porous materials such as activated carbons, even at very high pressure (>500 bar).[72] This is due to the physisorption nature of hydrogen uptake, which relies on weak adsorbate-adsorbent interactions between molecular H_2 and the adsorbent (carbon) surface. The amount of hydrogen stored may be increased if the uptake is performed at low temperature. Thus much work has been done on the hydrogen uptake of activated carbons at cryogenic temperature. The fact that gas physisorption at cryogenic temperature is mainly dependent on a large adsorbent surface marks out activated carbons as excellent candidates for cryogenic hydrogen storage. Thus, as a general rule, the cryogenic hydrogen uptake capacity of activated carbons depends on their surface area, with high surface area favoring higher uptakes. The available cryogenic hydrogen uptake data for activated carbons is clustered in two groups; at atmospheric pressure (1 bar) and at moderate pressure (10–100 bar) with the former ranging between 1 and 3 wt% and the latter in the range 2–7 wt%. The attraction and potential of cryogenic hydrogen storage is demonstrated by the study by Zhou and co-workers who found that storage of hydrogen in activated carbon at liquid nitrogen temperature is enhanced so as to reach a capacity of 4.1 kg H_2 per 100 L of storage vessel, and thus a gas pressure of 60 bar is needed compared to 150 bar for an empty vessel and 750 bar for the same container at room temperature.[341]

To date, a great deal of research effort has been expended in attempts to understand how the porosity of activated carbons affects hydrogen uptake in order to achieve appropriate gravimetric storage and volumetric uptake when considered in the context of the various targets set at levels that may allow commercial and practical

viability of hydrogen as a vehicular energy source. The targets that are often quoted are those set by the United States Department of Energy (DOE); the most recent targets for 2017 are a system gravimetric uptake capacity of 5.5 wt% and volumetric uptake capacity of 40 g/L.[262,342]

The uptake of activated carbons at cryogenic temperature is encouraging. Biomass-derived activated carbons have continued to attract attention. Their particular attraction is that the activation process turns low value waste into a useful activated carbon product. Examples include coffee bean waste-derived activated carbons, which have cryogenic hydrogen storage of 4.0 wt% at 40 bar.[297] The hydrogen storage capacity of the coffee bean-derived activated carbons show a linear relationship with the micropore volume, and exhibit a stored hydrogen density of 5.7 and 69.6 mg/cm^3 at room temperature and -196^{o}C, respectively. A series of biomass-derived activated carbons prepared by chemical activation of hemp (*Cannabis Sativa L.*) stem with KOH had surface area of 3241 m^2/g and total pore volume of 1.98 cm^3/g.[343] Hydrogen uptake of the carbons was found to be related to surface area, pore volume, and micropore volume, with the maximum hydrogen uptake being 3.3 wt% at −196°C and 1.0 bar.

Hydrothermally carbonized organic materials (furfural, glucose, starch, cellulose and eucalyptus sawdust) have been used as precursors to produce high-surface area (up to 2700 m^2/g) carbons, via two steps: i) hydrothermal carbonization of organic materials and ii) chemical activation with KOH as activating agent.[61] The activated carbon materials exhibit high hydrogen uptakes, up to 6.4 wt% (at -196^{o}C and 20 bar), and large isosteric heats of adsorption, up to 8.5 kJ/mol. Of particular interest for these carbons is the hydrogen storage density of between 12 and 16.4 μmol H_2/m^2. The hydrogen storage density was found to be closely related to the pore size of the carbons, with small micropores (ca. 1 nm) favouring a high density as shown in Figure 11.

Biomass waste-derived activated carbon generated from hydrolytic lignin exhibiting high surface area (2000−3100 m^2/g), large micropore volume (1.11−1.68 cm^3/g), and narrow pore size distribution (0.77−0.91 nm) was found to have hydrogen uptake of ca. 5 wt% with isosteric heat of adsorption of 4.1−7.5 kJ/mol.[344]

The on-going exploration of activated carbons as hydrogen stores is motivated by the need to achieve even higher hydrogen storage capacity than currently possible. The expectation is that improvements in the porosity of activated carbons, principally the surface area and targeted pore size, will lead to higher hydrogen storage capacity. Some in the research community have, however, questioned whether there is an unsurpassable upper limit for cryogenic hydrogen storage on activated carbons. Thus, Fierro et al. recently claimed that an apparent upper limit of 6.4 wt% hydrogen storage was observed in experimental work.[296] It was further claimed that such a limit is close to the theoretical limit of 6.8 wt% based on the maximum surface area achievable in activated carbons. Values close to the claimed upper limit have been achieved by anthracite derived activated carbons (i.e. 6.6 wt. % at -196^oC and 40 bar) in a study by Zhao and co-workers who assessed the effect of activation conditions on the storage capacity of anthracite activated carbons.[345,346] Activated carbons with surface area up to 3400 m^2/g and micropore volume of ca. 1 cm^3/g, achieved hydrogen storage capacity of up to 6.6 wt%, wherein both temperature and amount of activating agent (KOH) used were found to have a significant impact on hydrogen storage capacity mainly due to their effect on the textural properties. Nevertheless, as illustrated below, activated carbons can reach surface area higher than the apparent upper limit and achieve cryogenic hydrogen storage higher than the claimed maximum. It is now widely accepted that the actual hydrogen stored in activated carbon (and other types of porous materials) is dependent on several variables and not surface area alone.[347]

3.2.2.1 Double activation and supercritical fluid activation

As described above, chemical activation of carbonaceous materials (i.e., coal, biomass-derived products, etc.) constitutes an established route for the preparation of carbons with high surface area. In particular, activated carbons produced using KOH as activating agent exhibit several attractive properties: i) high surface area and large pore volume, ii) most of the porosity arises from uniform micropores in the 1–2 nm range, iii) the pore structure can be tailored by modifying the activating parameters (i.e., activation temperature and KOH/carbonaceous precursor weight ratio) and iv) the activation may be performed via an easy and one-step process. [49,64,348,349] In an attempt to enhance the hydrogen storage capacity of KOH activated carbons, Wang and co-workers, recently proposed a two-step procedure in which physical activation (with CO_2) was followed by a chemical (KOH) activation step.[68] This double activation protocol generates an activated carbon, with surface area of 3190 m^2/g, which exhibits hydrogen uptake of up to 7.08 wt% at -196ºC and 20 bar. This value is one of the highest hydrogen uptakes observed for activated carbons although the double activation protocol has the disadvantage of two steps, which is cumbersome. Apparently, the physical and chemical activation steps have different effects on the textural properties of the activated carbon with KOH activation generating most of the microporosity.[68] In a related study, activated carbon fibers, with surface area of up to 3144 m^2/g, were prepared from rayon-based carbon fibers via a two-step activation protocol incorporating the sequential use of steam and KOH.[295] The activated carbon fibers achieved a hydrogen storage capacity of 7.01 wt% at -196^{o}C and 40 bar, an uptake quite similar to that of Wang and co-workers mentioned above. Sevilla and co-workers have also observed high (up to 6.4 wt% at -196^{o}C and 20 bar) hydrogen uptake for doubly activated carbon derived from biomass.[61]

Other researchers have explored alternative avenues to enhancing the hydrogen uptake in activated carbons. For example, Salvador and co-workers studied the storage of hydrogen at -196^{o}C and 1.2 bar on carbon fibers activated with supercritical CO_2 and achieved an uptake of 2.45 wt%.[350] Based on the uptake data, the authors proposed a model of hydrogen storage based on adsorption on two different sites, namely (i) high-energy adsorbent-adsorbate interaction sites associated with very small micropores and (ii) lower-energy sites associated with larger pores. The model suggested that the activated carbon fibers adsorbed most of the hydrogen at low equilibrium pressures, and would virtually saturate at ca. 10 bar.

3.2.2.2 Polymer-derived activated carbons

Recently there have been attempts to obtain high surface area activated carbons using polymers as precursor *via* one-step activation procedures. Highly porous carbons have been successfully synthesized by chemical activation of polythiophene with KOH.[100] The porous carbons thus obtained possess high surface areas of up to 3000 m^2/g, and pore volumes of up to 1.75 cm^3/g, and sulfur content in the 3-12 wt% range. The hydrogen storage capacity of these S-doped activated carbons, at -196^{o}C and 20 bar, is up to 5.71 wt% with an estimated maximum hydrogen uptake of 6.64 wt%. Ultrahigh surface area (up to 3500 m^2/g) and pore volume (up to 2.6 cm^3/g) activated carbons can be obtained via chemical activation of polypyrrole with KOH.[99] The carbons achieve hydrogen storage capacity of up to 7.03 wt% at -196 ºC and 20 bar, which is the highest ever reported for one-step activated carbons as shown in Figure 12. The gravimetric hydrogen uptake of the carbons translates to very attractive volumetric density of up to 37 g H_2/L at 20 bar. The high gravimetric and volumetric capacity of the polypyrrole-derived carbons was due to the fact that their high porosity was not at the detriment of packing density. Activated carbons derived from mesoporous nitrogen-doped carbon

were explored as hydrogen stores at -196°C, achieving 6.84 wt% at 20 bar.[305] It was claimed that the hydrogen uptake capacity was related to both micropores and small mesopores of size between 2 and 3 nm, which suggested that small mesopores also make contributions to the hydrogen storage. A series of rectangular polyaniline tubes (RPTs) were activated with KOH generating activated carbons with surface area in the range 1680 to 2415 m^2/g and excess hydrogen uptake of up to 5.2 wt% at -196°C and 50 bar.[303] Such a hydrogen uptake is generally in line with the expected 1 wt% per 500 m^2/g. No mention was made in the report of any likely effect of the presence of nitrogen in the activated RPT carbons. Yang et al. reported the chemical activation of mesoporous carbon derived from mesoporous polymer to generate activated N-doped carbons with surface area of up to 2400 m^2/g and narrow pore size distribution. [351] The N-doped activated carbons exhibited hydrogen uptake capacity of up to 4.8 wt% at -196°C and 20 bar and remarkably high isosteric heat of adsorption for hydrogen 10 kJ/mol. The carbons contained only small amounts of nitrogen (0.2-1.1 wt%) and it was therefore not clear what role nitrogen atoms played in the uptake of hydrogen.

3.2.2.3 Activated carbide-derived carbons and zeolite templated carbons

Recently, several studies have reported on the post-synthesis chemical or physical activation of zeolite-templated carbons (ZTCs) or carbide-derived carbons (CDCs) with the aim of improving hydrogen storage capacity.[13,18,33,38,76, 352 , 353] Such multi-step (typically two steps) procedures can improve the hydrogen uptake by up to 96% and 63% for ZTCs and CDCs respectively. Thus, Sevilla et al. showed that chemical activation (with KOH) of ZTCs generates activated carbons with surface area in the range 1850 – 3100 m^2/g and pore volume of between 1.5 – 1.75 cm^3/g, which represents an increase of up to 84% in surface area and doubling of pore volume.[13] The activation results in an increase in hydrogen uptake capacity (at -196°C and 20 bar) of between 60

and 96% from 2.4–3.5 wt% for ZTCs to between 4.3 and 6.1 wt% for activated ZTCs as illustrated in Figure 13.

Regarding activation of CDCs, Gogotsi and co-workers, explored the effect of physical (with air and CO_2) and chemical (with KOH) activation of CDCs synthesized from TiC at different temperatures (400–1000ºC) on their hydrogen storage capacity.[18,38] Activation resulted in a two-fold increase in the surface area and pore volume of the CDCs, which reached 3360 m^2/g and 1.4 cm^3/g respectively. An enhancement in hydrogen uptake (at -196ºC and 60 bar) of up to 39% compared to the raw CDCs was observed reaching a value of 4.6 wt%. More recently, Sevilla and co-workers studied the influence of chemical activation on the porosity and hydrogen storage capacity of CDCs derived from zirconium carbide.[76] The resulting superactivated CDCs were still remarkably highly microporous, with typically 90% of surface area and 80% of pore volume associated with micropores, which resulted in an enhancement of up to 63% in hydrogen uptake capacity (Figure 14). The superactivated CDC with the highest surface area and pore volume values of (2770 m^2/g and 1.47 cm^3/g respectively) had a hydrogen uptake capacity of 6.2 wt% at -196^oC and 20 bar. Moreover, at 1 bar the superactivated CDCs store up to 2.7 wt% hydrogen, which is amongst the highest values ever reported for activated carbon.

The positive effects of activation with respect to hydrogen storage have also been demonstrated for MOF-templated carbons. A commercially available zeolitic imidazolate framework (ZIF), namely Basolite Z1200 (BASF), was used to nanocast ZIF-templated carbon with a surface area of ca. 1000 m^2/g and pore volume of ca. 0.7 cm^3/g.[354] Chemical activation (with KOH) of the ZIF-templated carbons increased their porosity by between 30 and 240% to achieve surface area and pore volume of 3200 m^2/g and 1.94 cm^3/g, respectively. The activation enhances the hydrogen uptake

capacity of the ZIF-templated carbons by between 25 and 140% from 2.6-3.1 wt% to the range 3.9-6.2 wt% (at -196^{o}C and 20 bar). Thus activation of certain types of porous carbons (ZTCs, CDCs or MOF-templated carbons) is a powerful tool for improving their performance as hydrogen stores by up to 100%. However, the effects of activation mean that a compromise between high surface area and total pore volume versus the micropore volume is essential for achieving optimised hydrogen storage.

3.2.2.4 Activated carbon aerogels

The surface area of carbon aerogels, a class of porous materials with a low bulk density, may be significantly increased via activation. Carbon aerogels are derived from a variety of precursors via three sequential steps; (i) sol-gel polymerization of molecular precursors into an organic gel, (ii) drying of the organic gel and (iii) carbonization of the organic gel to generate the final carbon aerogel. Baumann and co-workers prepared activated carbon aerogels with surface area as high as 3200 m^2/g and tested their hydrogen uptake at -196^{o}C.[355] The activation was performed using a stream of CO_2 at 950^{o}C. An unactivated carbon aerogel with surface area of 330 m^2/g adsorbed 0.8 wt% hydrogen at 20 bar, whereas the activated 3200 m^2/g sample stored 5.3 wt% hydrogen at 30 bar. In addition, an increase in the hydrogen uptake of unactivated carbon aerogels doped with Ni nanoparticles was observed. Overall, though, a linear relation was observed between hydrogen uptake and surface area as shown in Figure 15. The isosteric heat of hydrogen adsorption was calculated to be 7 kJ/mol for metal-doped carbon aerogels and 6 kJ/mol for activated carbon aerogels, which is comparable to other types of high surface area carbons.[356] Similar hydrogen uptake, i.e., 5.2 wt% at -196^{o}C and 35 bar was reported by Tian et al for KOH activated carbon aerogels.[357] Similar to the work of Baumann et al., a clear correlation was observed between the hydrogen uptake and surface area of the activated carbon aerogels. The successful synthesis of carbon

aerogels, via a simple subcritical drying route and subsequent activation to high surface area carbons with attractive properties for hydrogen storage has also been reported.[358] The unactivated carbon aerogels are highly microporous with a surface area of 508 m^2/g and pore volume of 0.68 cm^3/g wherein micropores account for 80% (407 m^2/g) of surface area. Chemical activation with KOH generates activated carbon aerogels with surface area of between 915 and 1980 m^2/g and pore volume of up to 2.03 cm^3/g. The activated carbon aerogels store between 3.5 and 4.3 wt% hydrogen at -196 ºC and 20 bar, and the amount of hydrogen adsorbed correlates well with the surface area. The hydrogen storage density of the carbons is high (up to 16.2 μmol H_2/m) with small micropores favouring high density.

3.3.3.5 Volumetric hydrogen uptake of activated carbons

Research in materials for hydrogen storage for on-board hydrogen storage systems, is geared towards achieving various targets set at levels that may allow commercial and practical viability. Targets that are often quoted are those set by the United States Department of Energy (DOE); the most recent targets for 2017 are a system gravimetric uptake capacity of 5.5 wt% and volumetric uptake capacity of 40 g/L.[262] It should thus be recognized that although most reports to date on hydrogen storage in activated carbons and other porous materials emphasize the gravimetric hydrogen uptake, it is the case that volumetric capacity is equally if not even more important. The conundrum is that the volumetric hydrogen uptake of a porous solid state material is related to its packing density. Most porous materials, including activated carbons, by their nature tend to have low density and therefore, despite attractive gravimetric hydrogen uptake, have low volumetric uptake.[31,261,263,359,360,361,362,363,364,365,366,367,368,369,370,371,372,373,374,375,376] For example, the total volumetric hydrogen storage on the best activated carbon at 25°C was found to be

16.7 g H_2/L and 37.2 g H_2/L at 200 bar and 500 bar, respectively and 38.8 g H_2/L at -196^{o}C and 40 bar.[68]

The volumetric hydrogen uptake of porous materials can potentially be improved by densification or compaction. However, such densification generally comes at the expense of surface area of the material, which rather negates any gains since the hydrogen uptake is dependent on surface area. [32,377,378,379,380,381,382] Recently, there have been studies that have considered the compaction behaviour of activated carbons (and metal organic frameworks) and its effect on hydrogen uptake.[383,384, 385, 386] In general, whilst activated carbons exhibit good mechanical stability,[383-385] MOFs tend to collapse and lose their porosity even at low compaction pressures.[385,386] There is ongoing interest in densification as a means of improving the hydrogen volumetric uptake capacity of activated carbons. High surface area activated carbons compacted at 40 MPa have been shown to have a packing density of 0.4 – 0.5 g/L and volumetric hydrogen uptake of ca. 20 g/L at -196^{o}C and 40 bar.[383,384] Linares-Solano and co-workers recently found that activated carbon monoliths with a high packing density of 0.7 g/cm^3 and good micropore volume can achieve a total volumetric hydrogen uptake capacity of ca. 39 g/L at -196^{o}C and 44 bar, which is amongst the highest values reported so far based on measured packing density of materials,[387] while Zhou and co-workers observed similar volumetric hydrogen uptake capacity of 41 g/L at -196^{o}C and 60 bar for compacted activated carbon with a packing density of 0.72 g/cm^3.[341] On the other hand, densification of zeolite Y-templated microporous carbons via hot-pressing at 300^{o}C and 147 MPa can achieve packing density of 0.7 – 0.9 g/cm^3, commercially available KOH-activated carbons do not undergo such densification when hot-pressed under similar conditions.[388] Thus, so far, attempts at densification of activated carbons have achieved a volumetric hydrogen uptake of no more than 40 g/L at 50 bar and -196^{o}C. [341, 383-388]

One of the limitations of further densification is that high surface area activated carbons can only withstand compaction pressure of up to 420 MPa.[385]

It has been suggested that the morphology and particle size of activated carbons may also play a role in the achievement of high volumetric hydrogen storage. In this regard, it has been claimed that activated polymer blend carbon nanofibers (ACNFs), due to their very thin diameter and amenability to packing together that allow high packing densities without change in textural properties, can store ca. 34 g H_2/L (for ACNFs with surface area of 1500–1700 m^2/g) at -196^{o}C and 40 bar.[389]

4. Summary and outlook

Activated carbons have a long history of usage and production, although their structural and chemical characteristics are experiencing continual evolution to fulfill the requirements of more demanding emergent applications. Research efforts are focused on advances in the control of their characteristics through the development of novel activation procedures and selection of precursors with specific chemical or structural characteristics. To date, activated carbons with high apparent surface area (up to ca. 4000 m^2/g) and various morphology (for example, powders, fibers, cloths, monoliths) have been synthesized through careful selection of activating agent and/or carbon precursor. Although certain activation procedures allow control and tuning of the pore size distribution, further advances are necessary because high surface areas are usually generated at the expense of pore size enlargement and general loss of pore size control.

In spite of the recent advances on the control of the porosity of carbon materials through templating procedures, and the development of novel materials, such as graphene or carbon nanotubes, activated carbons remain primary choice for the construction of electrodes for commercial supercapacitors due to their availability, cost and simpler production methods. The situation is likely to remain in the medium to long

term, although higher control over the textural properties (particularly pore size) is required to maximize the energy and power densities to comply with future energy demands. Furthermore, substantial reductions in cost are essential, and it is likely that precursors such as biomass, which is low-cost, readily available and renewable, will play a key role.

Activated carbons are being intensively studied for use in second generation supercapacitors, which promise to boost the amount of energy stored, while keeping the cycling stability and power capability to levels typical for EDLCs. With these novel configurations, the entire performance range (in terms of energy and power density) existing between conventional capacitors and electrochemical batteries will be covered. Furthermore, the possibility of using aqueous electrolytes, make these devices more economically and environmentally friendly than conventional EDLCs and batteries. These technologies are still in their infancy and will benefit from further breakthroughs in materials science, including in porous carbon fabrication, as well as in electrochemistry.

The development of porous materials capable of storing enough hydrogen to accomplish the targets required for on-board applications (mainly storage temperature and pressure) still remains a challenge. In this particular field of investigation, activated carbons are one of the most studied class of materials. However, the ambient temperature hydrogen storage capacity of activated carbons is, to date, well below the on-board targets. Although it is clear that optimization of the textural properties (surface area and pore size) can improve hydrogen storage at room temperature, real breakthroughs may not be possible via modification of textural properties alone. In this regard, a promising strategy to enhance the strength of hydrogen interaction with the sorbent so as to achieve hydrogen storage at room temperature is doping of activated carbons with

metal nanoparticles capable of producing spill-over. However, further fundamental research to clearly understand the spillover as applied in hydrogen storage processes is needed.

Acknowledgements

M.S. acknowledges the assistance of the Spanish MINECO for the award of a Ramón y Cajal contract.

Table 1. Supercapacitor performance of activated carbons present in the literature (two-electrode cell system).

Material	Electrolyte	Surface area (m^2/g)	Capacitance (F/g)[a]	E[b] (Wh/kg)	P[b] (kW/kg)	Reference
Rubber wood sawdust-based AC	H_2SO_4	< 920	8-139	~0.1	~0.6	129
ACF cloth	Organic	1500-2500	36.5	36.2	11.1	133
AC microbeads	KOH	606-2442	221-413	-	-	140
ACF			94-249	-	-	
ACF	Organic	682-771	41	-	-	142
ACs	Organic	960-1848	32	-	-	
ACs	Organic	1200-2315	60-125	-	-	112
ACs	H_2SO_4	505-1270[c]	65-322	-	-	143
Activated bituminous coal	H_2SO_4	800-3030	~160 – 310	-	-	145
	KOH		124-286			
	Organic		~120 – 180			
HTC-based AC	Organic	2125-2967	150 - 236	-	-	98
Straw-based AC	Organic	2316	251			146
Polypyrrole-based AC	Ionic Liquid	2095-3432	200 – 250 (20ºC) 250 – 300 (60ºC)	-	-	147
Coal and pitch-derived AC	H_2SO_4	1900-3150	198-312	-	-	148
PX-21	H_2SO_4	3000	240	-	-	148
Peach stone-derived AC	H_2SO_4	2692	279	-	-	149
	KOH		267			
Resorcinol/formaldehyde-based AC	KOH	522-2760	186-294	-	-	150
Mesophase-based AC	H_2SO_4	403-2652	50-334	0.45-2	1.5-12	127
Petroleum coke-based AC	KOH	792-2312	125-288	~8-10	0.2-0.3	151
MCMBs-based AC	KOH	2230-2543	248-326	-	-	152
Sunflower seed shell-based AC	KOH	619-2585	220-311	3-6	1-2.5	153
Petroleum coke-based AC	KOH	1180	160	8.7	-	154
Cherry stone-based AC	H_2SO_4	1130-1273	174-232	0.9-2	0.7-2	155
	Organic		110-120	4-7	1-6	
Beer lees-based AC	H_2SO_4	2113-3557	128-188	-	-	156
Needle coke-based AC	Organic	400-2900	14-44	-	-	157
Polyfurfuryl alcohol-derived AC	Organic	1070-2600	65-150	32	38	158
Mesophase pitch-based AC	Organic	687-2583	100-140	-	-	159
Black liquor-based AC	Organic	1370-3089	21-41.4	-	-	160
Anthracite-based AC	Organic	943-2479	57-167	-	-	161
PVDC-based AC	Organic	1829-2675	108-155	-	-	162
Sugar cane bagasse-based AC	H_2SO_4	1155-1788	240-300	5.9	10	163
Waste coffee ground-based AC	Organic	940-1021	100-134	5-40	0.1-21.5	164
Sucrose-based AC	Ionic liquids	817-1941	~45-178	-	-	165
CDC-based AC	Organic	1708-2139	103 - 180	-	-	102
Activated carbon aerogel	Organic	1408	100	27	-	166
Activated carbon aerogel	KOH	401-1418	71-146	-	-	167
Activated templated carbon	Organic	1178	93.5	-	-	168
Activated templated carbon	KOH	930-2060	120-180	~2.7-4.2	4.5-5.5	169
Activated templated carbon	H_2SO_4	1685	250	-	-	170
	Organic		~130			
Activated templated carbon	NaCl	1598, 1940	78.5, 114	-	-	171
Activated templated carbon	KOH	930-1410	144-200	-	-	172
Activated CNTs	KOH	~230-644	~20-55	-	-	173
Activated CNTs	KOH	510.5	50	-	-	174
Activated MEGO	Organic	3100	150	-	-	176
	Ionic liquid	2400	166	~70	~250	
Activated graphene-like nanosheets	KOH	1874	276	7.3	0.71	179
	Organic		196	54.7	10	

Activated carbon nanoplates	H_2SO_4	2557	264	~10	~100	180
	Ionic liquid		168	~15	217	
Activated sMEGO	Ionic liquid	3290	174	~74	338	182
O-rich activated anthracite and ACFs	H_2SO_4	173-3038	96-321[d]	-	-	48
O-rich activated mesophase pitch	H_2SO_4	1605-2008	~170-270	-	-	188
	KOH		~155-210			
O-rich corn grains-based AC	KOH	2936-3420	~205-257	-	-	190
O-rich bituminous coal-based AC	KOH	1950	370	8	10	191
O-rich AC	H_2SO_4	918-1480	227-351	-	-	193
O-doped AC	H_2SO_4	–	202-254	-	-	196
O-doped ACF	H_2SO_4	428-1011	112-180[d]			195
O-doped AC	Ionic liquid	-	126-130	-		197
	H_2SO_4		137			
O- and N-doped AC	H_2SO_4	1019	368	10	10	189
O- and N-doped ACs	H_2SO_4	808, 732	200, 230	-	-	192
O- and N-doped ACs	H_2SO_4	585-689	112-149	-	-	205
	KOH		96-109			
O and N-doped ACs	H_2SO_4	1577-2510	~200-350[d]	-	-	206
	KOH		~180-320[d]			
N-doped ACF	H_2SO_4	300-705	~170-200	4-6	20	200
	KOH		~220-240			
	Organic	705	~110	~5	30	
N-doped ACs	H_2SO_4	1364, 1435	260, 330	-	-	201
N-doped ACs	Organic	803-3075	~83-215	~4-9[e]	~0.4-0.8[e]	208
N-doped activated templated carbon	KOH	916	240	8	~1.5	209
S-doped AC	H_2SO_4	2420	206	-	-	210

[a] Determined at low current densities in charge/discharge experiments.
[b] Values at high current density.
[c] It is not BET surface area but total surface area estimated as $S_{mi}+S_{ex}$
[d] Values of capacitance for the three-electrode cell system.
[e] Expressed in volumetric base, i.e. E [=] Wh/L and P [=] kW/L.

Table 2. Supercapacitor performance of activated carbon/metal oxide composites or activated carbon/conducting polymer composites currently available in the literature (two-electrode cell system).

Material	Electrolyte	Surface area (m^2/g)	Capacitance (F/g)[a]	Reference
AC/RuO_2	H_2SO_4	529-2415	142-288	211
AC/RuO_2	H_2SO_4	845-1100	145-260[b]	212
AC/$RuO_2{\cdot}xH_2O$	H_2SO_4	-	243-350	213
AC/$RuO_2{\cdot}xH_2O$	H_2SO_4	460-878	135-250[b]	216
AC/RuO_2	KOH	-	218-288	217
AC/RuO_2	$TEABF_4$/AN	541-1094	~30-70	218
	EMIBF/AN		~50-80	
AC aerogel/Mn_3O_4	KOH	-	168[b]	220
AC-MCMB/MnO_2	$LiPF_6$ (EC+DMC)	-	183	221
AC-MCMB/Mn_3O_4	$LiPF_6$ (EC+DMC)	3127	178	222
AC/λ-MnO_2	Na_2SO_4	523, 1144	85, 120	223
AC-CNT/MnO_2	Na_2SO_4	-	250[b,c]	224
AC/MnO_2	Na_2SO_4	-	110-461[b]	225
AC/ZnO	Na_2SO_4	-	42-76[b]	226
AC/$Ni(OH)_2$	KOH	-	261-315[b]	227
AC/TiO_2	$LiClO_4$/EC-DEC or Et_4NBF_4/EC-DEC	-	64.5	228
AC/TiO_2	H_2SO_4	-	155	230
AC/PANI	H_2SO_4	-	~200-320[b]	231
AC/PANI	H_2SO_4	-	587[b]	232
AC/PANI	H_2SO_4	920-1127	273-316[b]	233
		903-1100	125-187[b]	
AC/PANI	H_2SO_4	875-2312	45-80	234
AC/PANI	H_2SO_4	-	238[b]	235
AC/PANI	H_2SO_4	-	180[b]	236

[a] Determined at low current densities in charge/discharge experiments.
[b] Values of capacitance for the three-electrode cell system.
[c] Determined at low sweep scan in CV experiments.

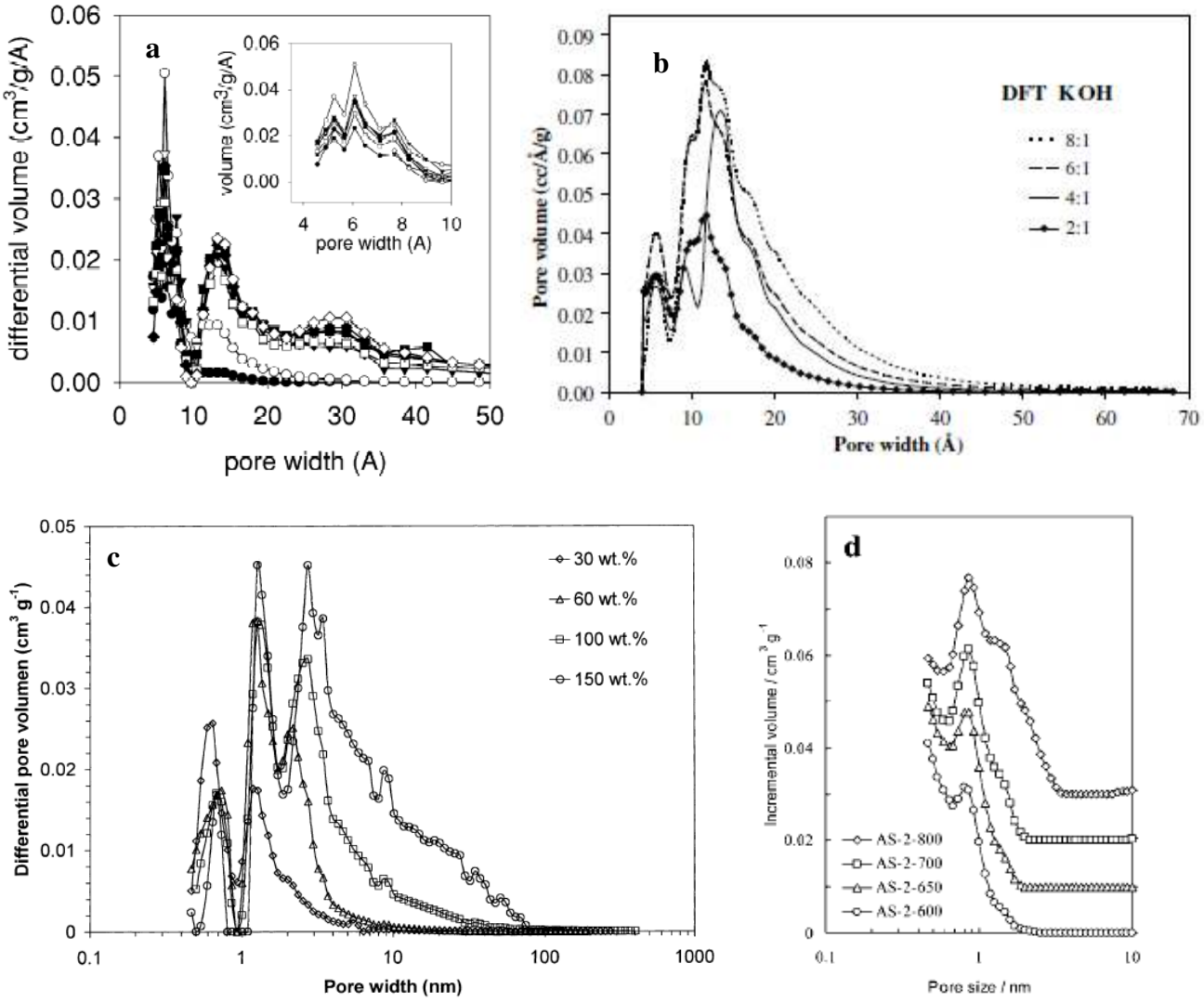

Figure 1. Pore size distribution of a) yarrabee1150 coal chars gasified to various conversions in air at 380ºC, determined from Ar adsorption isotherms at 87K (● - 4.5%, ○ - 15.4 %, ▼ - 40.4 %, ▽ - 57.0%, ■ - 57.3%, □ - 71.3%, ♦ - 83.1%, ◇ - 94.8 %) (reproduced with permission from ref. 16), b) activated carbons prepared at 750ºC using different KOH/precursor ratios (reproduced with permission from ref. 49), c) activated carbons prepared from coffee bean husks at 450ºC using different H_3PO_4/precursor ratios (reproduced with permission from ref. 50) and d) activated carbons prepared from hydrothermally carbonized eucalyptus sawdust at different activation temperatures (600-800ºC), using a KOH/HTC-sawdust ratio = 2 (reproduced with permission from ref. 62).

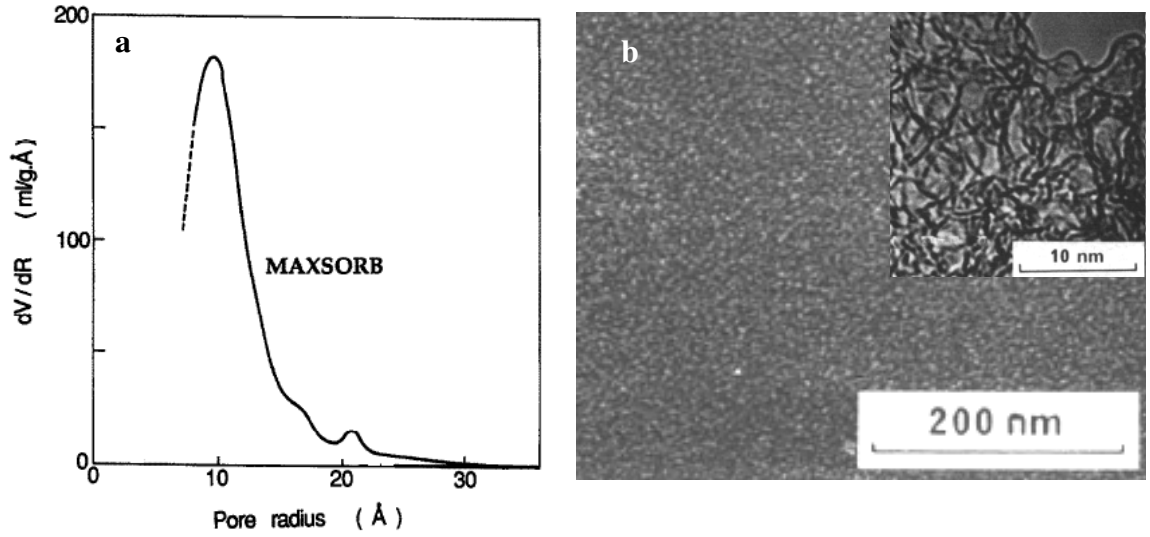

Figure 2. a) Pore size distribution of MAXSORB, KOH/C = 5, 700ºC for 100 min; adapted from ref. 88 and b) TEM micrograph of Amoco PX-21; reproduced with permission from ref. 87.

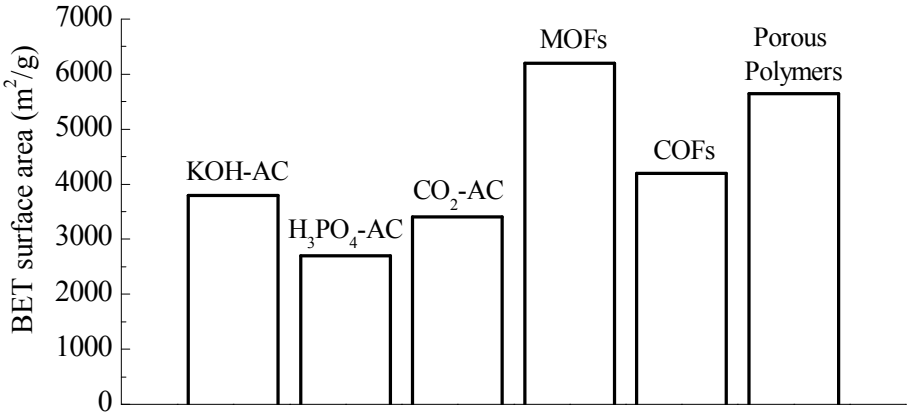

Figure 3. Comparison of the highest value of BET surface area reported for different types of porous materials: KOH-AC,[72] H_3PO_4-AC,[106] CO_2-AC,[18,33,] MOFs, [107] COFs,[109] porous polymers.[110]

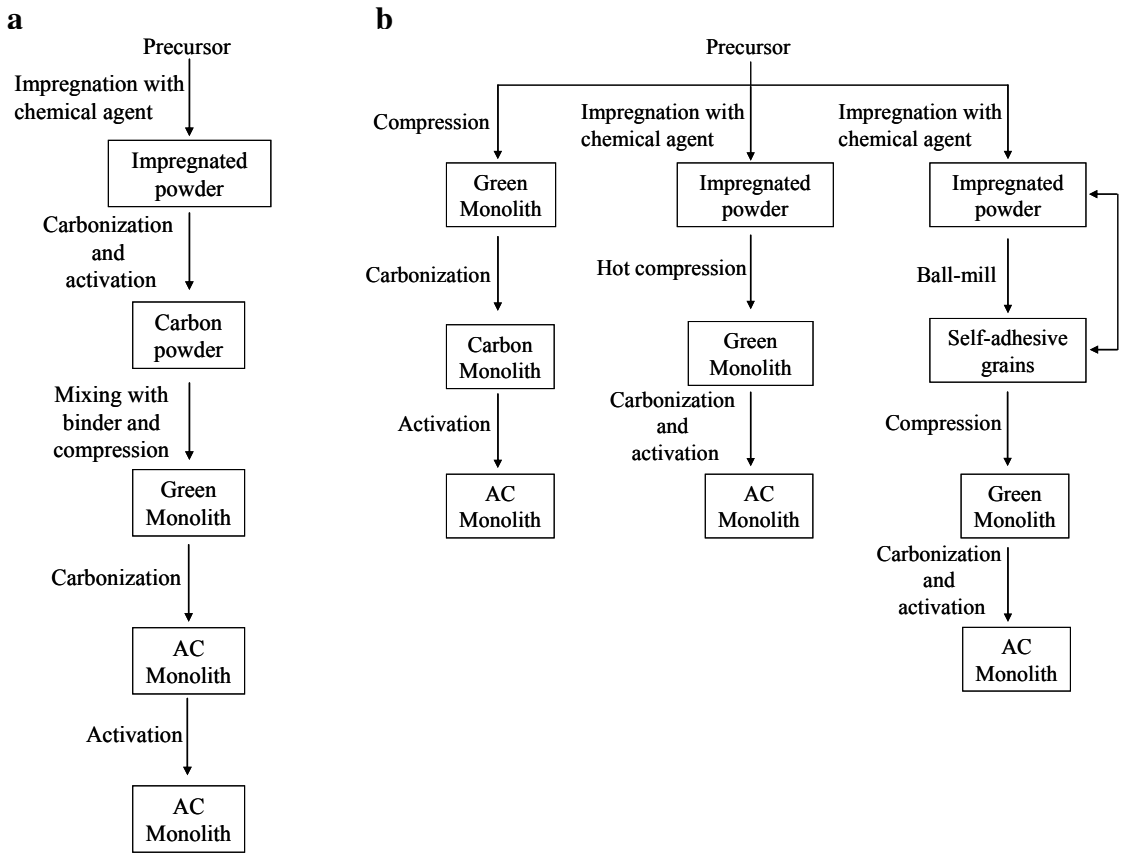

Figure 4. Synthesis procedures for the generation of activated carbon monoliths: a) with binder and b) binderless.

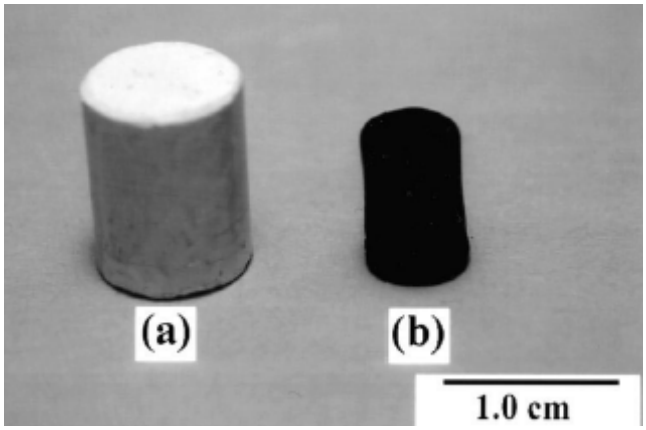

Figure 5. Photo image of the raw material (a) and activated carbon monolith (b). Reproduced with permission from ref. 119.

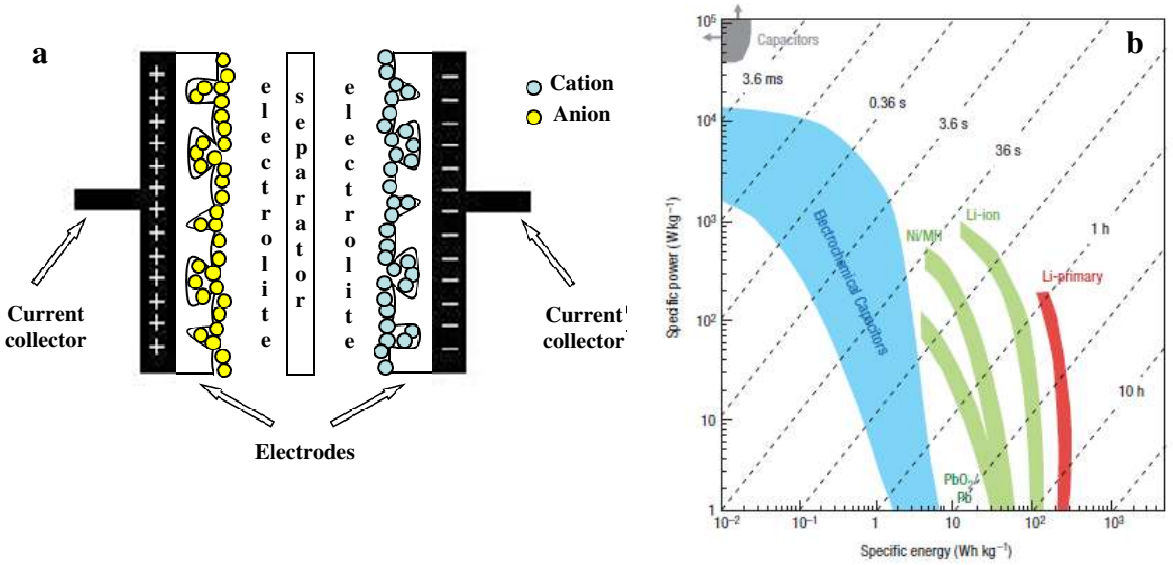

Figure 6. a) Schematic representation of a) a supercapacitor and b) Ragone plot for various electrical energy storage systems [Reproduced with permission from ref. 390].

Figure 7. Supercapacitors commercialized by different manufacturing companies.

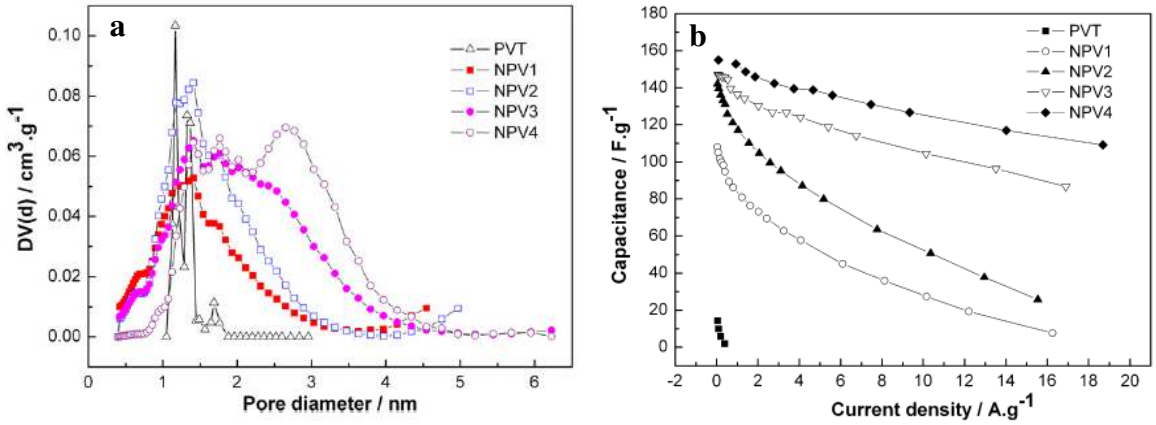

Figure 8. a) DFT-PSD of PVDC-derived char (PVT) and activated carbons prepared with different NaOH/precursor weight ratios (NPVr, r = NaOH/precursor weight ratio), and b) evolution of the specific capacitance of the various carbons with the increase of current density in galvanostatic charge-discharge experiments (Reproduced with permission from ref. 162)

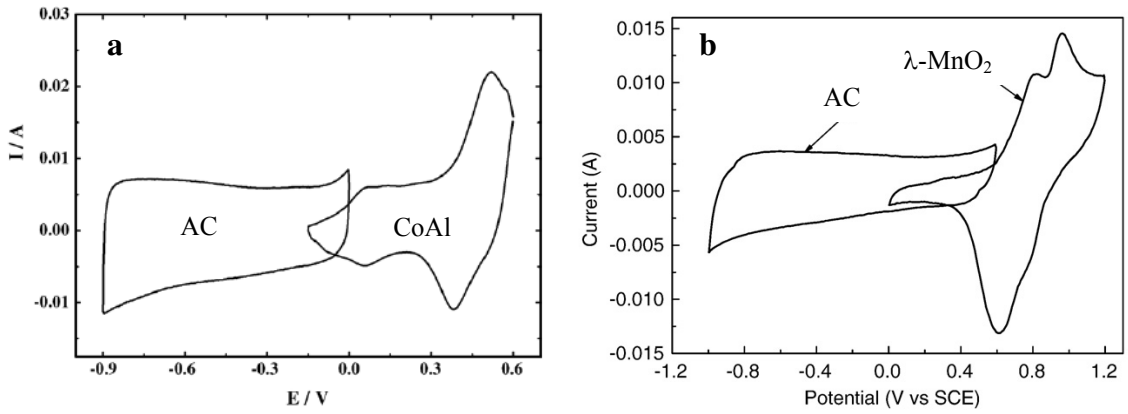

Figure 9. Cyclic voltammetry curves of a) AC and CoAl double hydroxide at a scan rate of 2 mV/s (reproduced with permission from ref. 238) and b) AC and λ-MnO_2 at a scan rate of 1 mV/s (reproduced with permission from ref. 241).

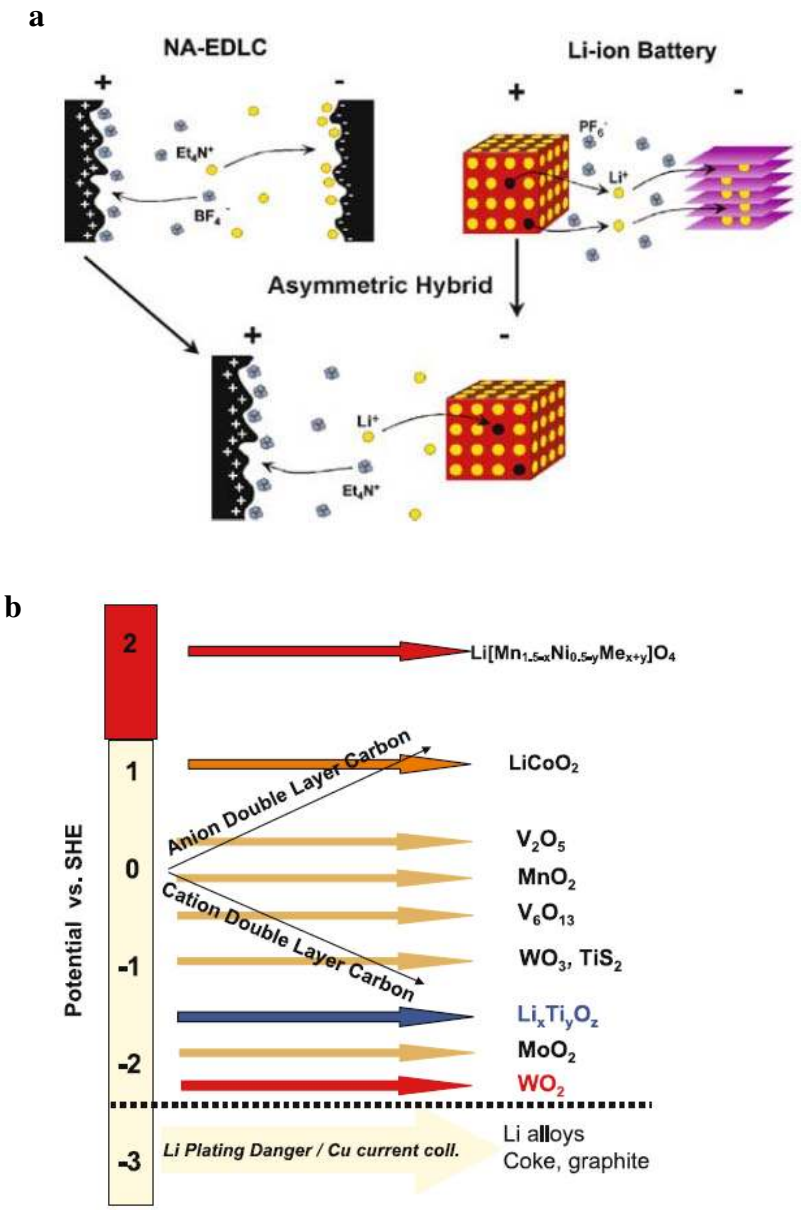

Figure 10. a) Schematic representation of the configuration of a non-aqueous Li-ion capacitor consisting of an AC positive electrode and a Li intercalation compound negative electrode and b) schematic illustration of the relative potentials of the positive and negative electrodes of EDLC based on AC as a function of charge and the general redox potential of various intercalation compounds. Reproduced both figures from ref. 237 with permission from Springer.

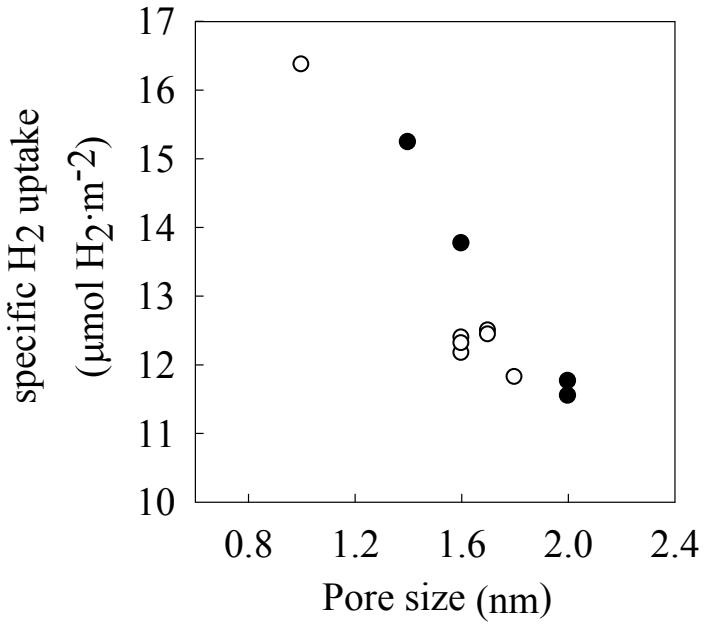

Figure 11. Plot of specific hydrogen uptake (in μmol H_2 m^{-2}) as a function of pore size for biomass-derived activated carbons; activated once (○) and doubly activated (●).[61]

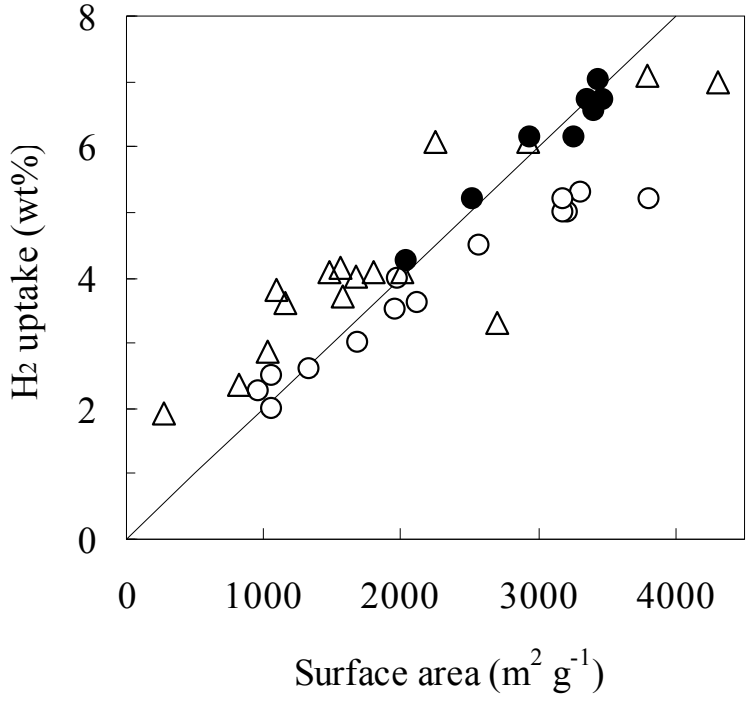

Figure 12. A comparison of the hydrogen uptake capacity (measured at -196 ºC and 20 bar) vs. surface area for one-step activated carbons and MOFs: Polypyrrole-derived activated carbons (●)[99] and data reported in the literature for a range of activated carbons (○), [61,72,376,391] and MOFs (Δ).[366] The solid line corresponds to the Chahine rule (i.e., 1 wt% sorption per 500 $m^2 g^1$).[392]

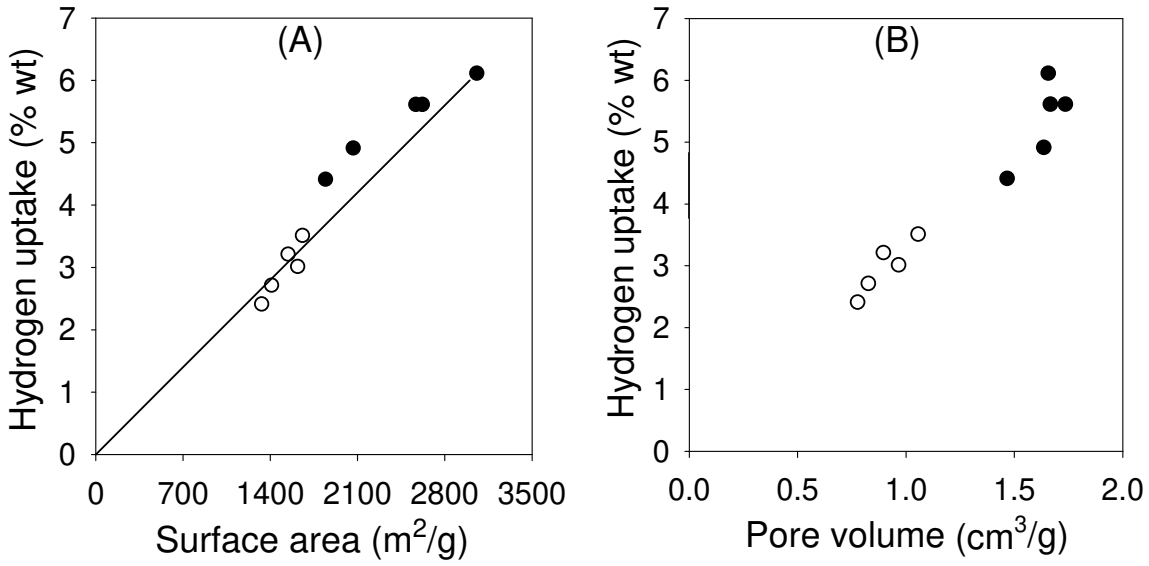

Figure 13. Plot of hydrogen storage capacity as a function of (A) surface area or (B) pore volume of zeolite-templated carbons (ZTCs) before (O) and after (●) chemical activation with KOH.[13] The line in (A) is corresponds to the Chahine rule.[392]

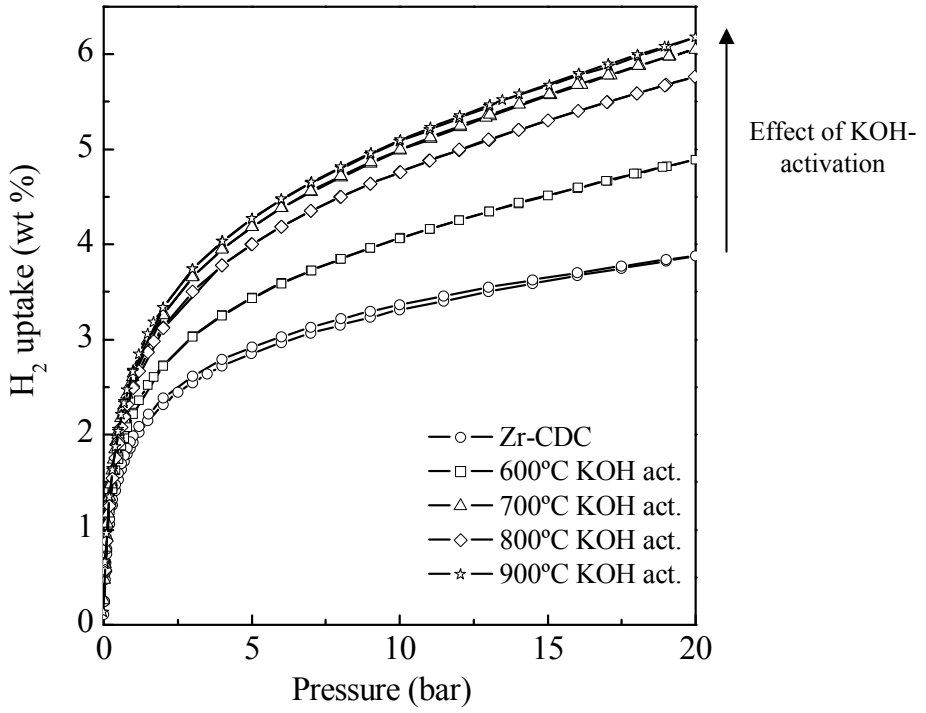

Figure 14. Hydrogen uptake isotherms at -196ºC in the pressure range 0-20 bar for a raw Zr-CDC before and after activation with KOH at various temperatures.[76]

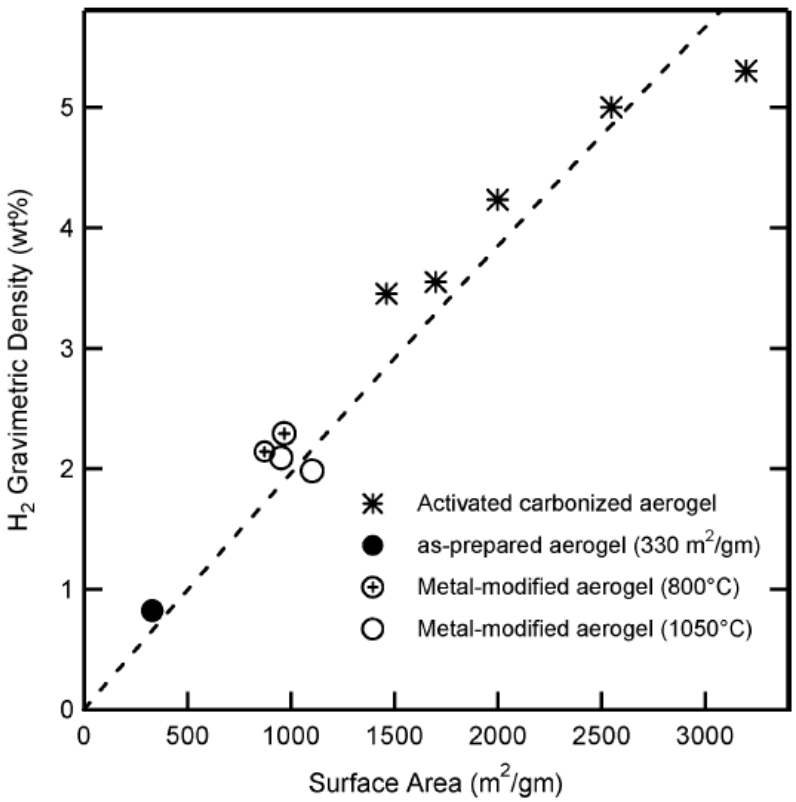

Figure 15. Hydrogen gravimetric density (wt%) saturation value at 77 K as a function of surface area for carbon aerogels before and after activation or metal implantation. The line represents the Chahine rule.[392] Reprinted with permission from ref. 355. Copyright 2006 American Chemical Society.

References

1 F. Çeçen and Ö. Aktas, in Activated Carbon for Water and Wastewater treatment, Ed. Wiley-VCH, Weinheim, 2011.
2 O. Ioannidou and A. Zabaniotou, *Renew. Sust. Energ. Rev*., 2007, **11**, 1966.
3 A. R. Mohamed, M. Mohammadi and G. N. Darzi, *Renew. Sust. Energ. Rev.*, 2010, **14**, 1591.
4 J. M. Dias, M. C. M. Alvim-Ferraz, M. F. Almeida, J. Rivera-Utrilla and M. Sánchez-Polo, *J. Environ. Manage*., 2007, **85**, 833.
5 P. A. Brown, S. A. Gill and S. J. Allen, *Wat. Res*., 2000, 34, 3907.
6 K. Y. Foo and B. H. Hameed, *Adv. Colloid Interfac*., 2009, **152**, 39.
7 J. M. Andrésen, C. E. Burgess, P. J. Pappano and H. H. Schobert, *Fuel Process. Technol.,* 2004, **85**, 1373.
8 R. Azargohar and A. K. Dalai, *Appl. Biochem. Biotech*., 2006, **131**, 762.
9 E. Raymundo-Piñero, D. Cazorla-Amorós, S. Delpeux, E. Frackowiak, K. Szostak and F. Beguin, *Carbon,* 2002, **40**, 1614.
10 E. Frackowiak, S. Delpeux, K. Jurewicz, K. Szostak, D. Cazorla-Amorós and F. Béguin, *Chem. Phys. Lett*., 2002, **361**, 35.
11 S. K. Ryu, H. Jin, D. Gondy, N. Pusset and P. Ehrburger, *Carbon*, 1993, **31**, 841.
12 S.-H. Yoon, S. Lim, Y. Song, Y. Ota, W. Qiao, A. Tanaka and I. Mochida, *Carbon*, 2004, **42**, 1723.
13 M. Sevilla, N. Alam and R. Mokaya, *J. Phys. Chem. C*., 2010, **114**, 11314.
14 F. Rodríguez-Reinoso and M. Molina-Sabio, *Carbon*, 1992, **30**, 1111.
15 E. A. Dawson, G. M. B. Parkes, P. A. Barnes and M. J. Chinn, *Carbon*, 2003, **41**, 571.
16 B. Feng and S. K. Bhatia, *Carbon*, 2003, **41**, 507.
17 J. Gañán, J. F. González, C. M. González-García, A. Ramiro, E. Sabio and S. Román, *Appl. Surf. Sci*., 2006, **252**, 5988.
18 S. Osswald, C. Portet, Y. Gogotsi, G. Laudisio, J. P. Singer, J. E. Fischer, V. V. Sokolov, J. A. Kukushkina and A. E. Kravchik, *J. Solid State Chem*., 2009, **182**, 1733.
19 F. Rodríguez-Reinoso, M. Molina-Sabio and M. T. González, *Carbon*, 1995, **3**, 15.
20 J. F. González, J. M. Encinar, C. M. González-García, E. Sabio, A. Ramiro, J. L. Canito and J. Gañán, *Appl. Surf. Sci*., 2006, **252**, 5999.
21 M. M. Johns, W. E. Marshall and C. A. Toles, *J. Chem. Technol. Biotechnol*., 1999, **74**, 1037.
22 C.-F. Chang, C.-Y. Chang and W.-T. Tsai, *J. Colloid Interface Sci*., 2000, **232**, 45.
23 G. San Miguel, G. D. Fowler and C. J. Sollars, *Carbon*, 2003, **41**, 1009.
24 A. Linares-Solano, C. S. Martinez de Lecea, D. Cazorla-Amorós and I. Martín-Gullón, *Energy Fuels*, 2000, **14**, 142.
25 S. Román, J. F. González, C. M. González-García and F. Zamora, *Fuel Process. Technol.,* 2008, **89**, 715.
26 J. F. González, S. Román, C. M. González-García, J. M. Valente Nabais and A. L. Ortiz, *Ind. Eng. Chem. Res*., 2009, **48**, 7474.
27 A. Singh and D. Lal, *J. Appl. Polymer Sci.,* 2010, **115**, 2409.
28 M. Molina-Sabio, M. T. González, F. Rodríguez-Reinoso and A. Sepúlveda-Escribano, *Carbon*, 1996, **34**, 505.
29 J. F. Byrne, H. Marsh, Introduction to carbon technology. In: Porosity in carbons, Ed. J. W. Patrick, London: Edward Arnold, 1995, 1.
30 M. G. Nijkamp, J. E. M. J. Raaymakers, A. J. van Dillen and K. P. de Jong, *Appl.*

Phys. A: Mater. Sci. Process., 2001, **72**, 619.
31 R. Ströbel, J. Garche, P. T. Moseley, L. Jörissen and G. Wolf, *J. Power Sources*, 2006, **159**, 781.
32 I. Cabria, M. J. López and J. A. Alonso, *Carbon*, 2007, **45**, 2649.
33 Y. Gogotsi, C. Portet, S. Osswald, J. M. Simmons, T. Yildirim, G. Laudisio and J. E. Fischer, *Int. J. Hydrogen Energy*, 2009, **34**, 6314.
34 G. Yushin, R. Dash, J. Jagiello, J. E. Fischer and Y. Gogotsi, *Adv. Funct. Mater*., 2006, **16**, 2288.
35 J. Chmiola, G. Yushin, Y. Gogotsi, C. Portet., P. Simon and P. L. Taberna, *Science*, 2006, **313**, 1760.
36 A. Janes and E. Lust, *J. Electrochem. Soc*., 2006, **153**, A113.
37 E. Raymundo-Pinero, K. Kierzek, J. Machnikowski and F. Beguin, *Carbon*, 2006, **44**, 2498.
38 J. Chmiola, C. Largeot, P.-L. Taberna, P. Simon and Y. Gogotsi, *Angew. Chem., Int. Ed*., 2008, **47**, 3392.
39 J. Chmiola, G. Yushin, R. Dash and Y. Gogotsi, *J. Power Sources*, 2006, **158**, 765.
40 M. Sevilla, P. Valle-Vigón and A. B. Fuertes, *Adv. Funct. Mater.,* 2011, **21**, 2781.
41 M. Jagtoyen and F. Derbyshire, *Carbon* 1998, 36, **7-8**, 1085.
42 M. Molina-Sabio and F. Rodriguez-Reinoso, *Colloids and Surfaces A: Physicochem. Eng. Aspects*, 2004, **241**, 15.
43 M.A. Lillo-Ródenas, D. Cazorla-Amorós and A. Linares-Solano, *Carbon*, 2003, **41**, 267.
44 M. A. Lillo-Ródenas, J. Juan-Juan, D. Cazorla-Amorós and A. Linares-Solano, *Carbon*, 2004, **42**, 1371.
45 D. Lozano-Castelló, J. M. Calo, D. Cazorla-Amorós and A. Linares-Solano, *Carbon*, 2007, **45**, 2529.
46 H. Teng and L.-Y. Hsu, *Ind. Eng. Chem. Res*., 1999, **38**, 2947.
47 C. Guan, K. Wang, C. Yang and X. S. Zhao, *Micropor. Mesopor. Mater*., 2009, **118**, 503.
48 M. J. Bleda-Martínez, J. A. Maciá-Agulló, D. Lozano-Castelló, E. Morallón, D. Cazorla-Amorós and A. Linares-Solano, *Carbon*, 2005, **43**, 2677.
49 J. A. Maciá-Agulló, B.C. Moore, D. Cazorla-Amorós and A. Linares-Solano, *Carbon*, 2004, **42**, 1367.
50 M. C. Baquero, L. Giraldo, J. C. Moreno, F. Suárez-García, A. Martínez-Alonso and J. M. D. Tascón, *J. Anal. Appl. Pyrolysis*, 2003, **70**, 779.
51 F. Rodríguez-Reinoso and M. Molina-Sabio, *Colloid Surface A*, 2004, **241**, 15.
52 H. Teng, T-S. Yeh and L-Y. Hsu, *Carbon*, 1998, **36**, 1387.
53 W. T. Tsai, C. Y. Chang and S. L. Lee, *Biores. Technol*., 1998, **64**, 211.
54 F. Suárez-García, A. Martıínez-Alonso and J. M. D. Tascón, *J. Annal. Appl. Pyrolysis*, 2002, **63**, 283.
55 L-Y. Hsu and H. Teng, *Fuel Process. Technol*., 2000, **64**, 155.
56 A. M. Puziy, O. I. Poddubnaya, A. Martínez-Alonso, F. Suárez-García and J. M. D. Tascón, *Carbon*, 2002, **40**, 1507.
57 M. J. Illán-Gómez, A. García-García, C. Salinas-Martínez de Lecea and A. Linares-Solano, *Energy Fuels*, 1996, **10**, 1108.
58 D. Lozano-Castelló, D. Cazorla-Amorós, A. Linares-Solano and D. F. Quinn, *Carbon*, 2002, **40**, 989.
59 P. M. Eletskii, V. A. Yakovlev, V. B. Fenelonov and V. N. Parmon, *Kinetics and Catalysis*, 2008, **49**, 708.

60 J. J. Niu and J. N. Wang, *Solid State Sci.,* 2008, **10**, 1189.
61 M. Sevilla, R. Mokaya and A. B. Fuertes, *Energy Environ. Sci*., 2011, **4**, 1400.
62 M. Sevilla and A. B. Fuertes, *Energy Environ. Sci*., 2011, **4**, 1765.
63 A. Ahmadpour and D. D. Do, *Carbon*, 1997, **35**, 1723.
64 D. Lozano-Castelló, D. Cazorla-Amorós and A. Linares-Solano, *Fuel Process. Technol.*, 2002, **77-78**, 325.
65 A. M. Puziy, O. I. Poddubnaya, A. Martínez-Alonso, F. Suárez-García and J. M. D. Tascón, *Carbon*, 2003, **41**, 1181.
66 A. W. M. Ip, J. P. Barford and G. McKay, *Biores. Technol*., 2008, **99**, 8909.
67 Q. Wenming, L. Licheng, Z. Qingfang and L. Lang, *J. Mater. Sci*., 1997, **32**, 4447.
68 H. Wang, Q. Gao and J. Hu, *J. Am. Chem. Soc*., 2001, **123**, 7016.
69 D. Lozano-Castelló, M. A. Lillo-Ródenas, D. Cazorla-Amorós and A. Linares-Solano, *Carbon*, 2001, **39**, 741.
70 D. Lozano-Castelló, D. Cazorla-Amorós and A. Linares-Solano, *Energy Fuels*, 2002, **16**, 1321.
71 Y. Guo, S. Yang, K. Yu, J. Zhao, Z. Wang and H. Xu, *Mater. Chem. Phys*., 2002, **74**, 320.
72 M. Jordá-Beneyto, F. Suárez-García, D. Lozano-Castelló, D. Cazorla-Amorós and A. Linares-Solano, *Carbon*, 2007, **45**, 293.
73 F. Zhang, H. Ma, J. Chen, G-D. Li, Y. Zhang and J-S. Chen, *Biores. Technol*., 2008, **99**, 4803.
74 F. Zhang, G-D. Li and J-S. Chen, *J. Colloid Interf. Sci*., 2008, **327**, 108.
75 Hale Sütcü and H. Demiral, *J. Anal. Appl. Pyrol*., 2009, **84**, 47.
76 M. Sevilla, R. Foulston and R. Mokaya, *Energy Environ. Sci*., 2010, **3**, 223.
77 J. C. Moreno-Piraján and L. Giraldo, *J. Anal. Appl. Pyrolysis*, 2010, **87**, 288.
78 R. Yavuz, H. Akyildiz, N. Karatepe and E Çetinkaya, *Fuel Process. Technol*., 2010, **91**, 80.
79 Z. Hu, H. Guo, M.P. Srinivasan and N.Yaming, *Sep. Purif. Technol*., 2003, **31**, 47.
80 M. J. Prauchner and F. Rodríguez-Reinoso, *Micropor. Mesopor. Mater*., 2008, **109**, 581.
81 A. Arami-Niya, W. M. A. W. Daud and F. S. Mjalli, *Chem. Eng. Res. Des*., 2011, **89**, 657.
82 F. Caturla, M. Molina-Sabio and F. Rodríguez-Reinoso, *Carbon*, 1991, **29**, 999.
83 M. Molina-Sabio, M. T. González, F. Rodríguez-Reinoso and A. Sepúlveda-Escribano, *Carbon*, 1996, **34**, 505.
84 F-C. Wu and R-L. Tseng, *J. Colloid Int. Sci*., 2006, **294**, 21.
85 Z. Hu and M. P. Srinivasan, *Micropor. Mesopor. Mater*., 2001, **43**, 267.
86 A. N. Wennerberg and T. M. O'Grady. US Patent 4,082,684 (1978)
87 H. Marsh, D.C. Crawford, T. M. O'Grady and A. N. Wennerberg, *Carbon*, 1982, **20**, 419.
88 T. Otowa, R. Tanibata and M. Itoh, *Gas Sep. Purif*., 1993, **7**, 241.
89 Y. Takeuchi , M. Hino, Y. Yoshimura, T. H. Izuhara and T. Nojima, *Gas Sep. Purif*., 1999, **15**, 79.
90 W.-C. Xu, K. Takahashi, Y. Matsuo, Y. Hattori, M. Kumagai, S. Ishiyama, K. Kaneko and S. Iijima, *Int. J. Hydrogen Energy*, 2007, **32**, 2504.
91 V. C. Menon and S. Komarneni, *J. Porous Mater*., 1998, **5**, 43.
92 D.F. Quinn, J.A. MacDonald and K. Sosin, *Amer. Chem. Soc. Preprints (Div. Fuel Chem.)*, 1994, **39**, 451.
93 Z. Yong, V. G. Mata and A. E. Rodrigues, *Adsorption*, 2001, B, 41.

94 G. C. Grunewald and R. S. Drago, *J. Molec. Catal*., 1990, **58**, 227.
95 G. C. Grunewald and R. S. Drago, *J. Am. Chem. Soc*., 1991, **113**, 1636.
96 T. A. Centeno and F. Stoeckli, *Electrochim. Acta*, 2006, **52**, 560.
97 V. Khomenko, E. Raymundo-Pinero and F. Béguin, *J. Power Sources*, 2006, **153**, 183.
98 L. Wei, M. Sevilla, A. B. Fuertes and R. Mokaya, G. Yushin, *Adv. Energy Mater*., 2011, **1**, 356.
99 M. Sevilla, R. Mokaya and A. B. Fuertes, *Energy Environ. Sci*., 2011, **4**, 2930.
100 M. Sevilla, A.B. Fuertes and R. Mokaya, *Int. J. Hydrogen Energy*, 2011, **36**, 15658.
101 S.-H. Yeon, S. Osswald, Y. Gogotsi, J. P. Singer, J. M. Simmons, J. E. Fischer, M. A. Lillo-Ródenas and A. Linares-Solano, *J. Power Sources*, 2009, **191**, 560.
102 C. Portet, M. A. Lillo-Ródenas, A. Linares-Solano, Y. Gogotsi, *Phys. Chem. Chem. Phys.*, 2009, **11**, 4943.
103 M. Choi and R. Ryoo, *J. Mater. Chem*., 2007, **17**, 4204.
104 K. Xia, Q. Gao, C. Wu, S. Song and M. Ruan, *Carbon*, 2007, **45**, 1989.
105 Y. Zhu, S. Murali, M. D. Stoller, K. J. Ganesh, W. Cai, P. J. Ferreira, A Pirkle, R. M. Wallace, K. A. Cychosz, M. Thommes, D. Su, E. A. Stach and R. S. Ruoff, *Scienc*e, 2011, **332**, 1537.
106 L. Wang, Y. Guo, B. Zou, C. Rong, X. Ma, Y. Qu, Y. Li and Z. Wang, *Biores. Technol*., 2011, **102**, 1947.
107 H. Furukawa, N. Ko, Y. B. Go, N. Aratani, S. B. Choi, E. Choi, A. O. Yazaydin, R. Q. Snurr, M. O'Keeffe, J. Kim and O. M. Yaghi, *Science*, 2010, **329**, 424.
108 J. R. Holst and A. I. Cooper, *Adv. Mater*., 2010, **22**, 5212.
109 H. M. El-Kaderi, J. R. Hunt, J. L. Mendoza-Cortes, A. P. Côté, R. E. Taylor, M. O'Keeffe and O. M. Yaghi, *Science*, 2007, **316**, 268.
110 T. Ben, H. Ren, S. Ma, D. Cao, J. Lan, X. Jing, W. Wang, J. Xu, F. Deng, J. M. Simmons, S. Qiu and G. Zhu, *Angew. Chem. Int. Ed*., 2009, **48**, 9457.
111 M. Yates, J. Blanco, P. Avila and M. P. Martin, *Micropor. Mesopor. Mater*., 2000, **37**, 201.
112 J. Gamby, P. L. Taberna, P. Simon, J. F. Fauvarque and M. Chesneau, *J. Power Sources*, 2001, **101**, 109.
113 S. Biloe, V. Goetz and S. Mauran, *Carbon*, 2001, **39**, 1653.
114 D. Lozano-Castelló, D. Cazorla-Amorós, A. Linares-Solano and D. F. Quinn, *Carbon*, 2002, **40**, 2817.
115 R. Ubago-Pérez, F. Carrasco-Marín, D Fairén-Jiménez and C. Moreno-Castilla, *Micropor. Mesopor. Mater*., 2006, **92**, 64.
116 M. S. Balathanigaimani, W.-G. Shim, J.-W. Lee and H. Moon, *Micropor. Mesopor. Mater.,* 2009, **119**, 47.
117 L. Giraldo and J. C. Moreno-Piraján, *Adsorpt. Sci. Technol*., 2009, **37**, 255.
118 J. Machnikowski, K. Kierzek, K. Lis, H. Machnikowska and L. Czepirski, *Energy Fuels*, 2010, **24**, 3410.
119 K. Inomata, K. Kanazawa, Y. Urabe, H. Hosono and T. Araki, *Carbon*, 2002, **40**, 87.
120 M. Molina-Sabio, C. Almansa and F. Rodríguez-Reinoso, *Carbon*, 2003, **41**, 2113.
121 C. Almansa, M. Molina-Sabio, F. Rodríguez-Reinoso, *Micropor. Mesopor. Mater*., 2004, **76**, 185.
122 D. P. Vargas-Delgadillo, L. Giraldo and J. C. Moreno-Piraján, *E-J. Chem*., 2010, **7**, 531.
123 A. A. García Blanco, J.C. Alexandre de Oliveira, R. López, J.C. Moreno-Piraján, L.

Giraldo, G. Zgrablich and K. Sapag, *Colloid Surface A*, 2010, **357**, 74.
124 D. P. Vargas, L. Giraldo, J. Silvestre-Albero and J. C. Moreno-Piraján, *Adsorption*, 2011, **17**, 497.
125 J. M. Ramos-Fernández, M. Martínez-Escanell and F. Rodríguez-Reinoso, *Carbon*, 2008, **46**, 365.
126 A. Whaby, J. M. Ramón-Fernández, M. Martínez-Escandell, A. Sepúlveda-Escribano, J. Silvestre-Albero and F. Rodríguez-Reinoso, *ChemSusChem*, 2010, **3**, 974.
127 V. Ruiz, C. Blanco, R. Santamaría, J. M. Ramos-Fernández, M. Martínez-Escandell, A. Sepúlveda-Escribano and F. Rodríguez-Reinoso, *Carbon*, 2009, **47**, 195.
128 M. Deraman, R. Omar, S. Zakaria, I. R. Mustapa, M. Talib, N. Alias and R. Jaafar, *J. Mater. Sci*., 2002, **37**, 3329.
129 E. Taer, M. Deraman, I. A. Talib, A. Awitdrus, S. A. Hashmi and A. A. Umar, *Int. J. Electrochem. Sci*., 2011, **6**, 3301.
130 G.-P. Hao, W.-C. Li, D. Qian, G.-H. Wang, W.-P. Zhang, T. Zhang, Q. Wang, F. Schüth, H.-J. Bongard and A.-H. Lu, *J. Am. Chem. Soc*., 2011, **133**, 11378.
131 H. E. Becker, U.S. Patent 2 800 616 (to General Electric) (1957).
132 http://www.kuraraychemical.com/Products/SC/capacitor.htm
133 M. Nawa, T. Nogami and H. Mikawa, *J. Electrochem. Soc*., 1984, **131**, 1457.
134 H. Yashima, T. Nogami and H. Mikawa, *Synthetic Metals*, 1985, **10**, 229.
135 H. Mikawa, T. Nogami and H. Yashima, *Molecular Crystals Liquid Crystals*, 1985, **121**, 259.
136 A. Yoshida, I. Tanahashi, Y. Takeuchi and A. Nishino, *IEEE Transactions on Components Hybrids and Manufacturing*, 1987, **10**, 100.
137 H. Nakagawa, A. Shudo and K. Miura, *J. Electrochem. Soc*., 2000, **147**, 38.
138 M. Morita, S. Watanabe, M. Ishikawa, H. Tamai and H. Yasuda, *Electrochem*., 2001, **69**, 462.
139 I. Tanahashi, *Electrochem. Solid State Lett*., 2005, **8**, A627.
140 H. Shi, *Electrochim. Acta*, 1996, 41, 1633.
141 D. Qu and H. Shi, *J. Power Sources*, 1998, 74, 99.
142 M. Endo, Y. J. Kim, T. Maeda, K. Koshiba, K. Katayam and M. S. Dresselhaus, *J. Mater. Res.*, 2001, **16**, 3402.
143 T. A. Centeno and F. Stoeckli, *Electrochim. Acta*, 2006, **52**, 560.
144 J. Huang, B. G. Sumpter and V. Meunier, *Chem. Eur. J*., 2008, **14**, 6614.
145 E. Raymundo-Piñero, K. Kierzek, J. Machnikowski and F. Béguin, *Carbon*, 2006, **44**, 2498.
146 X. Li, C. Han, X. Chen and C. Shi, *Micropor. Mesopor. Mater*., 2010, **131**, 303.
147 L. Wei, M. Sevilla, A. B. Fuertes, R. Mokaya and G. Yushin, *Adv. Funct. Mater*., 2011, **22**, 827.
148 K. Kierzek, E. Frackowiak, G. Lota, G. Gryglewicz and J. Machnikowski, *Electrochim. Acta*, 2004, **49**, 515.
149 M. Toupin, D. Belanger, I. R. Hill and D. Quinn, *J. Power Sources*, 2005, **140**, 203.
150 Y. Zhu, H. Hu, W. Li and X. Zhan, *Carbon*, 2007, **45**, 160.
151 X. He, Y. Geng, J. Qiu,, M. Zheng, S. Long and X. Zhan, *Carbon*, 2010, **48**, 1662.
152 L. Fuhu, C. Weidong,, S. Zengmin, W. Yixian and L. Yunfang and L. Hui, *Fuel Proces. Technol*., 2010, **91**, 17.
153 X. Li, W. Xing, S. Zhuo, J. Zhou, F. Li, S.-Z. Qiao and G.-Q. Lu, *Biores. Technol*., 2011, **102**, 1118.
154 X. Wang, D. Wang and J. Liang, *J. Mater. Sci. Technol*., 2003, **19**, 265.

155 M. Olivares-Marín, J. A. Fernández, M. J. Lázaro, C. Fernández-González, A. Macías-García,V. Gómez-Serrano, F. Stoeckli and T. A. Centeno, *Mater. Chem. Phys*., 2009, **114**, 323.
156 S. G. Lee, K. H. Park, W. G. Shim, M. S. Balathanigaimani and H. Moon, *J. Ind. Eng. Chem*., 2011, **17**, 450.
157 W. Qiao, S.-H. Yoon and I. Mochida, *Energy Fuels*, 2006, **20**, 1680.
158 V. Ruiz and A. G. Pandolfo, *Electrochim. Acta*, 2010, **55**, 7495.
159 D. Zhai, B. Li, H. Du, G. Wang and F. Kang, *J. Solid State Electrochem*., 2011, **15**, 787.
160 X.-Y. Zhao, J.-P. Cao, K. Morishita, J.-I. Ozaki and T. Takarada, *Energy Fuels*, 2010, **24**, 1889.
161 C.-X. Zhang, R. Zhang , B.-L. Xing,, G. Cheng, Y.-B. Xiea, W.-M. Qiao, L. Zhan, X.-Y. Liang and L.-C. Ling, *New Carbon Materials*, 2010, **25**, 129.
162 B. Xu, F. Wu, D. Mu, L. Dai, G. Cao, H. Zhang, S. Chen and Y. Yang, *Int. J. Hydrogen Energy*, 2010, **35**, 632.
163 T. E. Rufford, D. Hulicova-Jurcakova, K. Khosla, Z. Zhu and G. Q. Lu, *J. Power Sources*, 2010, **195**, 912.
164 T. E. Rufford, D. Hulicova-Jurcakova, E. Fised, Z. Zhu and G. Q. Lu, *Electrochem. Commun*., 2009, **11**, 974.
165 L. Wei and G. Yushin, *J. Power Sources*, 2011, **196**, 4072.
166 B. Fang, Y.Z. Wei, K. Maruyama and M. Kumagai, *J. Appl. Electrochem*., 2005, **35**, 229.
167 Y. Zhu, H. Hu, W.-C. Li and X. Zhang, *J. Power Sources*, 2006, **162**, 738.
168 J.-C. Zhao, C.-Y. Lai, Y. Dai and J.-Y. Xie, *J. Cent. South Univ. Technol*., 2005, **12**, 647.
169 W. Xing, C. C. Huang, S. P. Zhuo, X. Yuan, G. Q. Wang, D. Hulicova-Jurcakova, Z. F. Yan and G. Q. Lu, *Carbon*, 2009, **47**, 1715.
170 J. Jin, S. Tanaka, Y. Egashira and N. Nishiyama, *Carbon*, 2010, **48**, 1985.
171 X. Wang, J. S. Lee, C. Tsouris, D. W. DePaoli and S. Dai, *J. Mater. Chem*., 2010, **20**, 4602.
172 Y. Lv, F. Zhang, Y. Dou, Y. Zhai, J. Wang, H. Liu, Y. Xia, B. Tua and D. Zhao, *J. Mater. Chem*, 2012, **22**, 93.
173 B. Xu, F. Wu, Y. Sub, G. Cao, S. Chen, Z. Zhou and Y. Yang, *Electrochim. Acta*, 2008, **53**, 7730.
174 Q. Jiang, M. Z. Qu, G. M. Zhou, B. L. Zhang and Z. L. Yu, *Mater. Lett*., 2002, **57**, 988.
175 Q. Jiang, B. C. Liu, M. Z. Qu, G. M. Zhou, B. L. Zhang and Z. L. Yu, *Acta Chim. Sinica*, 2002, **60**, 1539.
176 Y. Zhu, S. Murali, M. D. Stoller, K. J. Ganesh, W. Cai, P. J. Ferreira, A. Pirkle, R. M. Wallace, K. A. Cychosz, M. Thommes, D. Su, E. A. Stach and R. S. Ruoff, *Science*, 2011, **332**, 1537.
177 Y Chen, X. Zhang, H. Zhang, X. Sun, D. Zhang and Y. Ma, *RSC Advances*, 2012, **2**, 7747.
178 L. L. Zhang, X. Zhao, M. D. Stoller, Y. Zhu, H. Ji, S. Murali, Y. Wu, S. Perales, B. Clevenger and R. S. Ruoff, *Nano Lett.*, 2012, **12**, 1806.
179 L. Sun, C. Tian, M. Li, X. Meng, L. Wang, R. Wang, J. Yin and H. Fu, *J. Mater. Chem. A., 2013,* **1**, 6462.
180 Y. S. Yun, S. Y. Cho, J. Shim , B. H. Kim, S.-J. Chang, S. J. Baek, Y. S. Huh, Y. Tak, Y. Woo Park, S. Park and H.-J. Jin, *Adv. Mater.* 2013, **25**, 1993–1998

181 H. Wang, Z. Xu, A. Kohandehghan, Z. Li, K. Cui, X. Tan, T. J. Stephenson, C. K. King'ondu, C. M. B. Holt, B. C. Olsen, J. K. Tak, D. Harfield, A. O. Anyia and D. Mitlin, *ACS Nano*, 2013, **7**, 5131.
182 T.Y. Kim, G. Jung, S. Yoo, K. S. Suh, and Rodney S. Ruoff, *ACS Nano*, 2013, **7**, 6899.
183 B. Zheng, T.-W. Chen, F.-N. Xiao,W.-J. Bao, X.-H. Xia, *J. Solid. State Electrochem.,* 2013, **17**, 1809.
184 C.-T. Hsieh and H. Teng, *Carbon*, 2002, **40**, 667.
185 S. Biniak, A. Swiatkowski and M. Makula, in Chemistry and Physics of Carbon (Ed: L. R. Radovic), Marcel Dekker, New York 2001, Ch. 3.
186 D. Qu, *J. Power Sources*, 2002, **109**, 403.
187 Y.-R. Nian and H. Teng, *J. Electroanal. Chem*., 2003, **540**, 119.
188 V. Ruiz, C. Blanco, E. Raymundo-Piñero, V. Khomenko, F. Béguin and R. Santamaría, *Electrochim. Acta*, 2007, **52**, 4969.
189 T. E. Rufford, D. Hulicova-Jurcakova,, Z. Zhu and G. Q. Lu, *Electrochem. Commun.,* 2008, **10**, 1594.
190 M.S. Balathanigaimani, W.-G. Shim, M.-J. Lee, C. Kim, J.-W. Lee and H. Moon, *Electrochem. Commun*., 2008, **10**, 868.
191 C. Zhang, D. Long, B. Xing, W. Qiao,, R. Zhang, L. Zhan, X. Liang and L. Ling, *Electrochem. Commun*., 2008, **10**, 1809.
192 D. Hulicova-Jurcakova, M. Seredych, G. Q. Lu and T. J. Bandosz, *Adv. Funct. Mater.,* 2009, **19**, 438.
193 S. Roldan, I. Villar, V. Ruíz, C. Blanco, M. Granda, R. Menéndez and R. Santamarıía, *Energy Fuels*, 2010, **24**, 3422.
194 D. Tashima,, E. Yamamoto, N. Kai, D. Fujikawa, G. Sakai, M. Otsubo and T. Kijima, *Carbon*, 2011, **49**, 4848.
195 J.-H. Lin,T.-H. Ko,Y.-H. Lin and C.-K. Pan, *Energy Fuels*, 2009, **23**, 4668.
196 M. J. Bleda-Martínez, D. Lozano-Castelló, E. Morallón, D. Cazorla-Amorós and A. Linares-Solano, *Carbon*, 2006, **44**, 2642.
197 R. Mysyk, E. Raymundo-Piñero, M. Anouti, D. Lemordant and F. Béguin, *Electrochem. Commun*., 2010, **12**, 414.
198 A. E. Ismanto, S. Wang, F. E. Soetaredjo and S. Ismadji, *Biores. Technol*., 2010, **101**, 3534.
199 G. Milczarek, A. Ciszewski and I. Stepniak, *J. Power Sources*, 2011, **196**, 7882.
200 E. J. Ra, E. Raymundo-Piñero, Y. H. Lee and F. Béguin, *Carbon*, 2009, **47**, 2984.
201 M. Seredych,, D. Hulicova-Jurcakova, G. Q. Lu and T. J. Bandosz, *Carbon*, 2008, **46**, 1475.
202 M. Abe, K. Kawashima, K. Kozawa, H. Sakai and K. Kaneko , *Langmuir*, 2006, **16**, 5059.
203 C. L.Mangun, K. R. Benak, J. Economy and K. L. Foster, *Carbon*, 2001, **39**, 1809.
204 W. Chen, F. S. Cannon and J. R. Rangel-Mendez, *Carbon*, 2005, **43**, 573.
205 K. Jurewicz, K. Babel, A. Ziolkowski and H. Wachowska, *Electrochim. Acta*, 2008, **48**, 1491.
206 R. Pietrzak,, K. Jurewicz, P. Nowicki, K. Babeł and H. Wachowska, *Fue*l, 2010, **89**, 3457.
207 J. R. Pels, F. Kapteijn, J. A. Moulijn, Q. Zhu and K. M. Thomas, *Carbon*, 1995, **33**, 1641.
208 Y. J. Kim, Y. Abe, T. Yanagiura, K. C. Park, M. Shimizu,T. Iwazaki, S. Nakagawa, M. Endo, M. S. Dresselhaus, Carbon, 2007, 45, 2116.

209 J. Jiang, Q. Gao, K. Xia, J. Hu, Micropor. Mesopor. Mater., 2009, 118, 28.
210 G. Hasegawa, M. Aoki, K. Kanamori, K. Nakanishi, T. Hanada and K. Tadanaga, *J. Mater. Chem*., 2011, **21**, 2060.
211 Y. Sato, K. Yomogida, T. Nanaumi, K. Kobayakawa, Y. Ohsawa and M. Kawai, *Electrochem. Solid State Lett*., 2000, **3**, 113.
212 M. Ramani, B. S. Haran, R. E. White, B. N. Popov and L. Arsov, *J. Power Sources*, 2001, **93**, 209.
213 J. Zhang, D. Jiang, B. Chen, J. Zhu, L. Jiang and H. Fang, *J. Electrochem. Soc*., 2001, **148**, A1362.
214 T. Nanaumi, Y. Ohsawa, K. Kobayakawa and Y. Sato, *Electrochemistry*, 2002, **70**, 681.
215 W.-C. Chen, C.-C. Hu, C.-C. Wang and C.-K. Min, *J. Power Sources*, 2004, **125**, 292.
216 M. S. Dandekar, G. Arabale and K. Vijayamohanan, *J. Power Sources*, 2005, **141**, 198.
217 Y.-F. Su, F. Wu, L.-Y. Bao and Z.-H.Yang, *New Carbon Materials*, 2007, **22**, 53.
218 X. J. He, Y.J. Geng, S. Oke,, K. Higashi, M. Yamamoto and H. Takikaw, *Synthetic Metals*, 2009, **159**, 7.
219 M. Egashira, Y. Marsuno, N. Yoshimoto and M. Morita, *J. Power Sources*, 2010, **195**, 3036.
220 Y. J. Lee, H. W. Park, S. Park and I. K. Song, *Curr. Appl. Phys*., 2012, **12**, 233.
221 Z.-S. Li, H.-Q. Wang, Y.-G. Huang, Q.-Y. Li and X.-Y. Wang, *Colloid Surface A*, 2010, **366**, 104.
222 H. Wang, Z. Li, J. Yang, Q. Li and X. Zhong, *J. Power Sources*, 2009, **194**, 1218.
223 A. Malak-Polaczyk, C. Matei-Ghimbeu, C. Vix-Guterl and E. Frackowiak, *J. Solid State Chem*., 2010, **183**, 969.
224 J. M. Ko and K. M. Kim, *Mater. Chem. Phys*., 2009, **114**, 837.
225 C.-C. Lin and C.-C. Yen, *J. Appl. Electrochem*., 2008, **38**, 1677.
226 M. Selvakumar, D. K. Bhat, A. M. Aggarwal, S. P. Iyer and G. Sravani, *Physica B*, 2010, **405**, 2286.
227 Q. Huang, X. Wang, J. Li, C. Dai, S. Gamboa and P. J. Sebastian, *J. Power Sources*, 2007, **164**, 425.
228 H. Liang, F. Chen, R. Li, L. Wang and Z. Deng, *Electrochim. Acta*, 2004, **49**, 3463.
229 Y. Huai, X. Hu, Z. Lin, Z. Deng and J. Suo, *Mater. Chem. Phys*, 2009, **113**, 962.
230 M.-K. Seo and S. J. Park, *J. Nanosci. Nanotechnol*., 2009, **9**, 7186.
231 Y.-R. Lin and H. Teng, *Carbon*, 2003, **41**, 2865.
232 Q. Wang Qin, J.-L. Li, F. Gao, W.-S. Li, K.-Z. Wu and X.-D. Wang, *New Carbon Materials*, 2008, **23**, 275.
233 M. J. Bleda-Martínez, E. Morallón and D. Cazorla-Amorós, *Electrochim. Acta*, 2007, **52**, 4962.
234 H. Tamai, M. Hakoda, T. Shiono and H. Yasuda, *J. Mater. Sci*., 2007, **42**,1293.
235 Z. H. Zhou, N. C. Cai, Y. Zeng and Y. H. Zhou, *Chinese J. Chem*., 2006, **24**, 13.
236 W.-C. Chen, T.-C. Wen, and H.Teng, *Electrochim. Acta*, 2003, **48**, 641.
237 I. Plitz, A. DuPasquier, F. Badway, J. Gural, N. Pereira, A. Gmitter, G. G.Amatucci, *Appl. Phys. A*, 2006, **82**, 615.
238 Y.-G. Wang, L.Cheng, Y.-Y. Xia, *J. Power Sources,* 2006, **153**, 191.
239 J. W. Lang, L. B. Kong, M. Liu, Y. C. Luo, Kang L, *J. Solid State Electrochem*., 2010, **14**, 1533.
240 V. Khomenko, E. Raymundo-Piñero, F. Béguin, *J Power Sources,* 2006, **153**, 183.

241 Y. Xue, Y. Chen, M.-L. Zhang, Y.-D. Yan, *Mater. Lett.,* 2008, **62**, 3884.
242 L. Demarconnay, E. Raymundo-Piñero, E. Béguin, *J. Power Sources*, 2011, **196**, 580.
243 Z. J. Fan, J. Yan, T. Wei, L. J. Zhi, G. Q. Ning, T. Y. Li, F. Wei, *Adv. Funct. Mater*., 2011, **21**, 2366.
244 A. D. Fabio, A. Giorgi, M. Mastragostino, and F. Soavi, *J. Electrochem. Soc.*, 2001, **148**, A845.
245 A. Laforgue, P. Simon, J. F. Fauvarque, J. F. Sarrau, and P. Lailler, *J. Electrochem. Soc.*, 2001, **148**, A1130.
246 A. Laforgue, P. Simon, J. F. Fauvarque, M. Mastragostino, F. Soavi, J. F. Sarrau, P. Lailler, M. Conte, E. Rossi, and S. Saguattie, *J. Electrochem. Soc.*, 2003, **150**, A645.
247 G. G. Amatucci, F. Badway, A. DuPasquier, and T. Zheng, *J. Electrochem. Soc.*, 2001, **148**, A930
248 T. Brousse, R. Marchand, P.-L. Taberna, P. Simon, J. Power Sources, 2006, **158**, 571.
249 V. Aravindan, W. Chuilinga and S. Madhavi, *J. Mater. Chem*., 2012, **22**, 16026.
250 K. Kim, M.-S. Kim and T. Yeu, *Bull. Korean Chem. Soc.,* 2010, **31**, 3183.
251 M. Mladenov, K. Alexandrova, N. V. Petrov, B. Tsyntsarski, D. Kovacheva, N. Saliyski and R. Raicheff, *J Solid State Electrochem,* 2013 **17**, 2101.
252 Y.-G. Wang, Y.-Y. Xia, *Electrochem. Commun.*, 2005, **7**, 1138.
253 J. Zheng, Proc. the 18th International Seminar on Double Layer Capacitors and Similar Energy Storage Device, Deerfield Beach, Florida, 2008.
254 J. Zheng, Proc. the 12th International Seminar on Double Layer Capacitors and Similar Energy Storage Device, Deerfield Beach, Florida, 2002.
255 J. Zheng, X. Wang, Proc. the 13th International Seminar on Double Layer Capacitors and Similar Energy Storage Device, Deerfield Beach, Florida, 2003.
256 J.P. Zheng, *J. Electrochem. Soc*., 2009, **156**, A500.
257 J.P. Zheng, *J. Electrochem. Soc*., 2003, **150**, A484.
258 J. Yan, Y. Sun, L. Jiang, Y. Tian, R. Xue, L. Hao, W. Liu, B. Yi., *J. Renew. Sustain. Ener.,* 2013, **5**, 021404.
259 W. C van den Berg and C. O. Arean, *Chem. Commun.,* 2008, **6**, 668.
260 L. Schlapbach and A. Zuttel, *Nature*, 2001, **414**, 353.
261 D. Zhao, D. Yuan and H. C. Zhou, *Energy Environ. Sci.,* 2008, **1**, 222.
262 DOE Hydrogen Program, FY 2004 Progress Report. <http://www.eere.energy.gov/hydrogenandfuelcells/pdfs/annual04/iii_storage_intro.pdf>. 179-181 (2004).
263 L. J. Murray, M. Dinca and J. R. Long, *Chem. Soc. Rev*. 2009, **38**, 1294.
264 X. Lin, J. H. Jia, P. Hubberstey, M. Schroder, and N. R. Champness, *Cryst. Eng. Comm.*, 2007, **9**, 438.
265 D. J. Collins and H. C. Zhou, *J. Mater. Chem*. 2007, **17**, 3154.
266 S. Sculley, D. Q. Yuan and H. C. Zhou, *Energy Environ. Sci*. 2011, **4**, 2721.
267 M. Hirscher, B. Panella and B. Schmitz, *Micropor. Mesopor. Mater.,* 2010, **129**, 335.
268 R. E. Morris and P. Wheatley, *Angew. Chem. Int. Ed.,* 2008, **47**, 4966.
269 J. X. Dong, X. Y. Wang, H. Xu, Q. Zhao and J. Li, *Int. J. Hydrogen Energy,* 2007, ***32***, 4998.
270 J. Weitkamp, M. Ftritz and S. Ernst, *Int. J. Hydrogen Energy*, 1995, **12**, 967.
271 Y. W. Li and R. T. Yang, *J. Phy. Chem. B*, 2006, **110**, 17175.

272 Z. Yang, Y. Xia and R. Mokaya, *J. Am. Chem. Soc.,* 2007, **129**, 1673.
273 A. Pacula and R. Mokaya, *J. Phys. Chem. C,* 2008, **112**, 2764.
274 N. Alam and R. Mokaya, *Energy Environ. Sci*., 2010, **3**, 1773.
275 Z. Yang, Y. Xia, X. Sun and R. Mokaya, *J. Phys. Chem. B,* 2006, **110**, 18424.
276 L. Chen, R. K. Singh and P. Webley, *Micropor. Mesopor. Mater.,* 2007, **102**, 159.
277 Y. Xia, Z. Yang and R. Mokaya, *Chem. Vap. Deposition*, 2010, **16**, 322.
278 N. Alam and R. Mokaya, *Micropor. Mesopor. Mater.,* 2011, **142**, 716.
279 N. Alam and R. Mokaya, *Micropor. Mesopor. Mater.,* 2011, **144**, 140.
280 Y. Xia, G. S. Walker, D. M. Grant, R. Mokaya, *J. Am. Chem. Soc*. 2009, **131**, 16493.
281 J. C. Wang, M. Oschatz, T. Biemelt, L. Borchardt, I. Senkovska, M. R. Lohe, S. Kaskel, *J. Mater. Chem*., 2012, **22**, 23893.
282 Y. Gogotsi, R. K. Dash, G. Yushin, T. Yildirim, G. Laudisio and J. E. Fischer, *J. Am. Chem. Soc.,* 2005, ***127***, 16006.
283 M. Oschatz, L. Borchardt, I. Senkovska, N. Klein, M. Leistner, S. Kaskel, *Carbon*, 2013, **55**, 139.
284 A. Nikitin and Y. Gogotsi, in Encyclopedia of Nanoscience and Nanotechnology, Vol. 10: Nanostructured carbide-derived carbons (Ed.: H.S. Nalwa) Pages 1-22, 2004
285 C. Carpetis and W. Peschka, *Int. J. Hydrogen Energy*, 1980, **5**, 539.
286 R. K. Agarwal, J. S. Noh, J. A. Schwarz and P. Davini, *Carbon*, 1987, **25**, 219.
287 J. S. Noh, R. K. Agarwal and J. A. Schwarz, *Int. J. Hydrogen Energy*, 1987, **12**, 693.
288 J. A. Schwarz, J. S. Noh and R. K. Agarwal, Selection and treatment of activated carbon - to enhance their storage capacity for hydrogen and other gases. US Patent 4960450-A.
289 J. A. Schwarz, Storage of hydrogen - using storage medium comprising activated carbon combined with a transition metal, Patent; EP230384-A; JP62216901-A; US4716736-A; EP230384-B; DE3778039-G; JP96022721-B2.
290 K. A. G. Amankwah and J. A. Schwarz, *Int. J. Hydrogen Energy*, 1991, **16**, 339.
291 P. Benard and R. Chahine, *Int. J. Hydrogen Energy*, 2001, **26,** 849.
292 M. A. de la Casa-Lillo , F. Lamari-Darkrim, D. Cazorla-Amorós, and A. Linares-Solano *J. Phys. Chem. B*, 2002, **106**, 10930.
293 N. Texier-Mandoki, J. Dentzer, T. Piquero, S. Saadallah, P. David and C. Vix-Guterl, *Carbon* 2004, **42**, 2744.
294 H. Jin, Y. S. Lee, and I. Hong, *Catal. Today*, 2007, **120**, 399.
295 F. Gao, D. L. Zhao, Y. Li and X. G. Li, *J. Phys. Chem. Solids*, 2010, **71**, 444.
296 V. Fierro, A. Szczurek, C. Zlotea, J. F. Mareche, M. T. Izquierdo, A. Albiniak, M. Latroche, G. Furdin and A. Celzard, *Carbon*, 2010, **48**, 1902.
297 H. Akasaka, T. Takahata, I. Toda, H. Ono, S. Ohshio, S. Himeno, T. Kokubu and H. Saitoh, *Int. J. Hydrogen Energy*, 2011, **36**, 580.
298 V. V. Bhat, C. I. Contescu, N. C. Gallego and F. S. Baker, *Carbon*, 2010, **48**, 1331.
299 Y. Sun and P. A. Webley, *Chem. Eng. J*., 2010, **162**, 883.
300 S. U. Rather, R. Zacharia, M.-u. -d. Naik, S. W. Hwang, A. R. Kim and K. S. Nahm, *Int. J. Hydrogen Energy*, 2008, **33**, 6710.
301 V. Jiménez, P. Sánchez, J. Antonio Díaz, J. Luis Valverde and A. Romero, *Chem. Phys. Lett.,* 2010, **485**, 152.
302 J. S. Im, S.-J. Park, T. J. Kim, Y. H. Kim and Y.-S. Lee, *J. Colloid Interface Sci*., 2008, **318**, 42.

303 Y. Chen, H. Zhu and Y. Liu, *Int. J. Hydrogen Energy*, 2011, **36**, 11738.
304 B.-J. Kim, Y.-S. Lee and S.-J. Park, *Int. J. Hydrogen Energy*, 2008, **33**, 2254.
305 Z. Zheng, Q. Gao and J. Jiang, *Carbon*, 2010, **48**, 2968.
306 M. Sankaran and B. Viswanathan, *Carbon*, 2006, **44**, 2816.
307 M. Sankaran, B. Viswanathan and S. S. Murthy, *Int. J. Hydrogen Energy*, 2008, **33**, 393.
308 Z. Zhou, X. Gao, J. Yan and D. Song, *Carbon*, 2006, **44**, 939.
309 Z. H. Zhu, H. Hatori, S. B. Wang and G. Q. Lu, *J. Phys. Chem. B*, 2005, **109**, 16744.
310 Z. Zhou, X. Gao, J. Yan and D. Song, *Carbon*, 2006, **44**, 939.
311 Z. H. Zhu, H. Hatori, S. B. Wang and G. Q. Lu, *J. Phys. Chem. B*, 2005, **109**, 16744.
312 C.-C. Huang, H.-M. Chen, C.-H. Chen and J.-C. Huang, *Sep. Purif. Technol*., 2010, **70**, 291.
313 X. B. Zhao, B. Xiao, A. J. Fletcher and K. M. Thomas, *J. Phys. Chem. B*, 2005, **109**, 8880.
314 C. Zlotea, F. Cuevas, V. R. Paul-Boncour, E. Leroy, P. Dibandjo, R. Gadiou, C. Vix-Guterl and M. Latroche, *J. Am. Chem. Soc.*, 2010, **132**, 7720.
315 D. Giasafaki, A. Bourlinos, G. Charalambopoulou, A. Stubos and T. Steriotis, *Micropor. Mesopor. Mater.*, 2012, **154**, 74.
316 C.-H. Chen and C.-C. Huang, *Micropor. Mesopor. Mater.*, 2008, **109**, 549.
317 C.-Y. Chen, J.-K. Chang, W.-T. Tsai and C.-H. Hung, *J. Mater. Chem.*, 2011, **21**, 19063.
318 X. R. Ye, Y. Lin and C. M. Wai, *Chem. Commun.*, 2003, 642.
319 R. Zacharia, K. Y. Kim, A. K. M. Fazle Kibria and K. S. Nahm, *Chem. Phys. Lett.*, 2005, **412**, 369.
320 N. P. Stadie, J. J. Purewal, C. C. Ahn and B. Fultz, *Langmuir*, 2010, **26**, 15481.
321 R. Campesi, F. Cuevas, E. Leroy, M. Hirscher, R. Gadiou, C. Vix-Guterl and M. Latroche, *Micropor. Mesopor. Mater.*, 2009, **117**, 511.
322 R. B. Levy and M. Boudart, *J. Catal.*, 1974, **32**, 304.
323 S. J. Teichner, *Appl. Catal.*, 1990, **62**, 1.
324 V. V. Bhat, C. I. Contescu and N. C. Gallego, *Nanotechnology*, 2009, **20**, 204011.
325 R. Prins, *Chem. Rev.*, 2012, **112**, 2714.
326 C. S. Tsao, Y. Liu, M. Li, Y. Zhang, J. B. Leao, H. W. Chang, M. S. Yu and S. H. Chen, *J. Phys. Chem. Lett.*, 2010, **1**, 1569.
327 C. S. Tsao, Y. Liu, H. Y. Chuang, H. H. Tseng, T. Y. Chen, C. H Chen, M. S. Yu, Q Li, A. Lueking, and S. H Chen, *J. Phys. Chem. Lett.,* 2011, **2**, 2322.
328 C. I. Contescu, C. M. Brown, Y. Liu, V. V. Bhat and N. C. Gallego, *J. Phys. Chem. C*, 2009, **113**, 5886.
329 C. S. Tsao, Y. R. Tzeng, M. S. Yu, C. Y. Wang, H. H. Tseng, T. Y. Chung, H. C. Wu, K. Yamamoto, K. Kaneko and S. H. Chen, *J. Phys. Chem. Lett.*, 2010, **1**, 1060.
330 Y. Li and R. T. Yang, *J. Phys. Chem. C*, 2007, **111**, 11086.
331 Y. Li and R. T. Yang, C. J. Liu and Z. Wang, *Ind. Eng. Chem. Res.*, 2007, **46**, 8277.
332 M. Zieliński, R. Wojcieszak, S. Monteverdi, M. Mercy and M. M. Bettahar, *Int. J. Hydrogen Energy*, 2007, **32**, 1024.
333 M. Zieliński, R. Wojcieszak, S. Monteverdi, M. Mercy and M. M. Bettahar, *Catal. Commun.,* 2005, **6**, 777.
334 L. F. Yang, C. L. Xie, C. F. Hu, M. T. Zheng, H. B. Wang, J. H. Cui, Y. Xiao, B. F. Lei, Y. L. Liu and L. X. Sun, *Australian J. Chem.*, 2013, **66**, 548.

335 A. Anson, E. Lafuente, E. Urriolabeitia, R. Navarro, A. M. Benito, W. K. Maser and M. T. Martinez, *J. Phys. Chem. B* **2006**, *110*, 6643.
336 W. Zhao, V. Fierro, C. Zlotea, M.T. Izquierdo, C. Chevalier-César, M. Latroche, A. Celzard, *Int. J. Hydrogen Energy*, 2012, **37**, 5072.
337 M. Ohno, N. Okamura, T. Kose, T. Asada and K. Kawata, *J. Porous Mater.,* 2012, **19**, 1063.
338 J. S. Im, O. Kwon, Y. H. Kim, S.-J. Park and Y.-S. Lee, *Micropor. Mesopor. Mater.,* 2008, **115**, 514.
339 H. Y. Tian, C. E. Buckley, D. A. Sheppard, M. Paskevicius and N. Hanna, *Int. J. Hydrogen Energy*, 2010, **35**, 13242.
340 S. Y. Lee, S. J. Park and S. J. Park, *Int. J. Hydrogen Energy*, 2011, **36**, 8381.
341 L. Zhou, Y. Zhou and Y. Sun, *Int. J. Hydrogen Energy,* 2004, **29**, 319.
342 U.S. Department of Energy Website: https://www1.eere.energy.gov /hydrogenandfuelcells/storage/current_technology.html
343 R. Yang, G. Q. Liu, M. Li, J. Zhang, X. Hao, *Micropor. Mesopor. Mater*., 2012, **158**, 108.
344 F. Cheng, J. Liang, J. Zhao, Z. Tao and J. Chen, *Chem. Mater.*, 2008, **20**, 1889.
345 W. Zhao, V. Fierro, C. Zlotea, E. Aylon, M. T. Izquierdo, M. Latroche and A. Celzard, *Int. J. Hydrogen Energy*, 2011, **36**, 11746.
346 W. Zhao, V. Fierro, C. Zlotea, N. Fernandez-Huerta, M. T. Izquierdo and A. Celzard, *Int. J. Hydrogen Energy*, 2012, **37**, 14278.
347 E. Masika and R. Mokaya, *J. Phys. Chem. C*, 2012, **116**, 25734.
348 S. J. Allen, L. Whitten and G. Mckay, *Dev. Chem. Eng. Mineral Process*., 1998, **6**, 231.
349 M. Wu, Q. Zha, J. Qiu, Y. Guo, H. Shang and A. Yuan, *Carbon,* 2004, **42**, 205.
350 F. Salvador, M. J. Sanchez-Montero, J. Montero and C. Izquierdo, *J. Power Sources*, 2009, **190**, 331.
351 Z. Yang, Y. Xia, Y. Zhu, *Mater. Chem. Phys*., 2013, **141**, 318.
352 K. Xia, Q. Gao, S. Song, C. Wu, J. Jiang, J. Hu and L. Gao, *Int. J. Hydrogen Energy,* 2008, ***33***, 116.
353 M. Armandi, B. Bonelli, E. I. Karaindrou, C. Otero Area and E. Garrone, *Catal. Today,* 2008, ***138***, 244.
354 A. Almasoudi and R. Mokaya, *J. Mater. Chem.,* 2012, **22**, 146.
355 H. Kabbour, T. F. Baumann, J. H. Satcher, A. Saulnier and C. C. Ahn, *Chem. Mater*., 2006, **18**, 6085.
356 P. Benard and R. Chahine, *Langmuir*, 2001, **17**, 1950.
357 H. Y. Tian, C. E. Buckley, S. B. Wang, M. F. Zhou, *Carbon*, 2009, **47**, 2128.
358 C. Robertson and R. Mokaya, *Micropor. Mesopor. Mater.,* 2013, **179**, 151.
359 H. K. Chae, D. Y. Siberio-Perez, J. Kim, Y. Go, M. Eddaoudi, A. J. Matzger, M. O'Keeffe and O. M Yaghi, *Nature*, 2004, **427**, 523.
360 N. L. Rosi, J. Eckert, M. Eddaoudi, D. T. Vodak, J. Kim, M. O'Keeffe and O. M. Yaghi, *Science*, 2003, **300**, 1127.
361 J. L. C. Rowsell and O. M. Yaghi, *Angew. Chem. Int. Ed.*, 2005, **44**, 4670.
362 J. L. C. Rowsell, A. R. Millward, K. S. Park and O. M. Yaghi, *J. Am. Chem. Soc.*, 2004, **126**, 5666.
363 S. Q. Ma and H. C. Zhou, *Chem. Commun.*, 2010, **46**, 44.
364 Y. H. Hu and L. Zhang, *Adv. Mater.*, 2010, **22**, 117.
365 S. S. Han, J. L. Mendoza-Cortes and W. A. Goddard, *Chem. Soc. Rev*., 2009, **38**, 1460.

366 K. M. Thomas, *Dalton Trans.*, 2009, 1487.
367 P. Chen, X. Wu, J. Lin and K. L. Tan, *Science*, 1999, **285**, 91.
368 C. Liu, Y. Y. Fan, M. Liu, H. T. Cong, H. M. Cheng and M. S. Dresselhaus, *Science,* 1999, **286**, 1127.
369 C. C. Ahn, Y. Ye, B. V. Ratnakumar, C. Witham, R. C. Bowman and B. Fultz, *Appl. Phys. Lett.*, 1998, **73**, 3378.
370 G. G. Tibbetts, G. P. Meisner and C. H. Olk, *Carbon* 2001, **39**, 2291.
371 M. Ritschel, M. Uhlemann, O. Gutfleisch, A. Leonhardt, A. Graff, C. Taschner and J. Fink, *Appl. Phys. Lett.*, 2002, **80**, 2985.
372 H. M. Cheng, Q. H. Yang and C. Liu, *Carbon*. 2001, **39**, 1447.
373 M. Hirscher and B. Panella, *J. Alloys Compd*, 2005, **404**, 399.
374 A. C. Dillon and M. J. Heben, *Appl. Phys. A: Mater. Sci. Process*. 2001, **72**, 133.
375 A. Zuttel, P. Sudan, P. Mauron, T. Kiyobayashi, C. Emmenegger and L. Sclapbach, *Int. J. Hydrogen Energy,* 2002, **27**, 203.
376 K. M. Thomas, *Catal. Today*, 2007, **120**, 389.
377 Y. Xia and R. Mokaya, *J. Phys. Chem. C*, 2007, **111**, 10035.
378 J. Pang, J. E. Hampsey, Z. Wu, Q. Hu and Y. Lu, *Appl. Phys. Lett*., 2004, **85**, 4887.
379 E. Terres, B. Panella, T. Hayashi, Y. A. Kim, M. Endo, J. M. Dominguez, M. Hirscher, H. Terrones and M. Terrones, *Chem. Phys. Lett.*, 2005, **403**, 363.
380 B. Fang, H. Zhou and I. Honma, *J. Phys. Chem. B*, 2006, **110**, 4875.
381 M. Sevilla and R. Mokaya, *J. Mater. Chem.,* 2011, **21**, 4727.
382 Y. Xia, Z. Yang and R. Mokaya, *Nanoscale*, 2010, **2**, 639.
383 J. P. Marco-Lozar, J. Juan-Juan, F. Suárez-García, D. Cazorla-Amorós and A. Linares-Solano, *Int. J. Hydrogen Energy*, 2012, **37**, 2370.
384 J. Juan-Juan, J. P. Marco-Lozar, F. Suárez-García, D. Cazorla-Amorós and A. Linares-Solano, *Carbon*, 2010, **48**, 2906.
385 J. Alcañiz-Monge, G. Trautwein, M. Pérez-Cadenas and M. C. Román-Martínez, *Microp. Mesop. Mater.*, 2009, **126**, 291.
386 K. W. Chapman, G. J. Halder and P. J. Chupas, *J. Am. Chem. Soc.*, 2009, **131**, 17546.
387 M. Jordá-Beneyto, D. Lozano-Castelló, F. Suárez-García, D.Cazorla-Amorós and A. Linares-Solano, *Micropor. Mesopor. Mater*., 2008, **112**, 235.
388 P. X. Hou, H. Orikasa, H. Itoi, H. Nishihara and T. Kyotani, *Carbon*, 2007, **45**, 2011.
389 F. Suárez-García, E. Vilaplana-Ortego, M. Kunowsky, M. Kimura, A. Oya and A. Linares-Solano, *Int. J. Hydrogen Energy*, 2009, **34**, 9141.
390 P. Simon, and Y. Gogotsi, *Nature Mater*., 2008, **7**, 845.
391 B. Panella, M. Hirscher and S. Roth, *Carbon,* 2005, **43**, 2209.
392 E. Poirier, R. Chahine and T. K. Bose, *Int. J. Hydrogen Energy,* 2001, **26**, 831.